Supporting Information
Unexpected Precatalyst σ-Ligand Effects in Phenoxyimine Zr-Catalyzed Ethylene/1-Octene Copolymerizations

Yanshan Gao,[1] Matthew D. Christianson,[2] Yang Wang,[1] Jiazhen Chen,[1] Steve Marshall,[2] Jerzy Klosin,[2]* Tracy L. Lohr,[1]*‡ and Tobin J. Marks[1]*

[1]Department of Chemistry, Northwestern University, Evanston, IL 60208–3113, USA.
[2]Corporate R&D, The Dow Chemical Company, 1776 Building, Midland, Michigan 48674, USA.

‡ Current Address: Shell Catalysts & Technologies, Shell Technology Center Houston, 3333 Highway 6 South, Houston, Texas, 77082, USA

*E-mails: t-marks@northwestern.edu; tracy.lohr@shell.com; jklosin@dow.com

Contents

Materials and Methods

All manipulations of air-sensitive materials were performed with rigorous exclusion of O_2 and moisture in oven-dried Schlenk-type glassware on a dual manifold Schlenk line, interfaced to a high-vacuum line (10^{-6} Torr), or in a N_2-filled MBraun glove box with a high-capacity recirculator (<1 ppm O_2). Argon (Airgas, pre-purified grade) was purified by passage through a supported MnO oxygen-removal column and an activated Davison 4 Å molecular sieve column. Ethylene (Airgas) was purified by passage through an oxygen/moisture trap (Matheson, model MTRP-0042-XX). Hydrocarbon solvents (*n*-pentane and toluene) were dried using activated alumina columns according to the method described by Grubbs[1] and were additionally vacuum-transferred from Na/K alloy immediately before vacuum line manipulations. C_6D_6 and C_7D_8 (Cambridge Isotope Laboratories, 99+ atom %D) were stored over Na/K alloy in vacuum and vacuum transferred immediately prior to use. The solvents 1,2-difluorobenzene (DFB) and $CDCl_3$ were distilled from CaH_2 and stored over activated Davison 4 Å molecular sieves. All other reagents, including 1,1,2,2-tetrachloroethane-d_2, were used as received.

Physical and Analytical Measurements

NMR spectra were recorded on Varian UNITY Inova-500 (FT, 500 MHz, ^{1}H; 125 MHz, ^{13}C), UNITY Inova-400 (FT, 400 MHz, ^{1}H; 100 MHz, ^{13}C), Agilent DD2-HCN600 (FT, 600 MHz, ^{1}H; 150 MHz, ^{13}C) or Bruker ASCEND-400 (FT, 400.13 MHz, ^{1}H; 100.60 MHz, ^{13}C). Chemical shifts for ^{1}H and ^{13}C spectra were referenced using internal solvent resonances and are reported relative to tetramethylsilane (TMS). NMR experiments on air-sensitive samples were conducted in Teflon valve-sealed sample tubes (J-Young). Elemental analyses (CHN) were performed by Midwest Microlab, Indianapolis, Indiana. ^{13}CNMR analysis of polymer microstructure were conducted in 1,1,2,2-tetrachloroethane-d_2 at 120 °C with delay time (d_1) = 10 sec. Signals were assigned according to the literature for these polymers.[2] High temperature Gel Permeation Chromatography (GPC) for samples in Table 1 of the manuscript was was carried out in 1,2,4-trichlorobenzene (stabilized with 125 ppm of BHT) at 150 °C on a Polymer Laboratories 220 instrument equipped with a set of three PLgel 10μm mixed-B columns with differential refractive index, viscosity, and light scattering (15° and 90°) detectors. Data reported were determined via triple detection. High temperature GPC analysis for samples in Table 2 of the manuscript was performed using a PolymerChar GPC with infrared detector (IR5) and a set of four Agilent PLgel MIXED-A columns. Octene incorporation for samples in Table 2 of the manuscript was determined by comparing the methyl and methylene signals recorded by the GPC IR5 detector using a linear calibration from co-polymers of known composition.

Synthesis of the Ligand and Complexes

1) Synthesis of FI-H Ligand

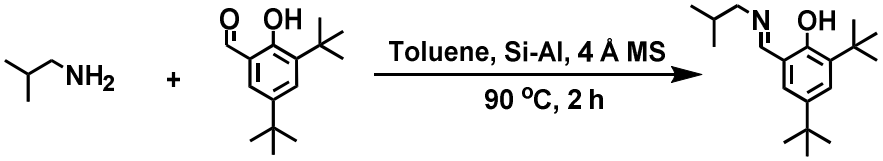

3,5-Di-tert-butyl-2-hydroxybenzaldehyde (3.86 g, 16.5 mmol, 1.0 equiv), **isobutyl amine** (3.65 g, 50.0 mmol, 3.03 equiv), silicon-alumina, and 4Å molecular sieves were combined in anhydrous toluene (50 mL) in a 100-mL round bottom flask. The reaction was then heated to 90 °C for 2 h. After the reaction period, the solution was filtered through celite, and the filtrate was concentrated to dryness and kept under high vacuum overnight to yield the product as a dark yellow solid (4.67 g, 98% yield). ^{1}H NMR (400 MHz, $CDCl_3$) δ 13.98 (s, 1H), 8.32 (s, 1H), 7.38 (d, J =

2.4 Hz, 1H), 7.09 (d, J = 2.4 Hz, 1H), 3.41 (dd, J = 6.5, 1.2 Hz, 2H), 1.46 (s, 9H), 1.32 (s, 9H), 0.99 (d, J = 6.7 Hz, 6H). ^{13}C NMR (101 MHz, $CDCl_3$) δ 165.86, 158.45, 139.94, 136.82, 126.80, 125.84, 118.02, 67.74, 35.19, 34.27, 31.67, 29.82, 29.59, 20.71. Elem. Anal. Calcd for $C_{19}H_{31}NO$: C 78.84, H 10.80, N 4.84; Found: C 78.77, H 10.69, N 4.89

2) Synthesis of the Complex $FI_2Zr(NMe_2)_2$ (1)

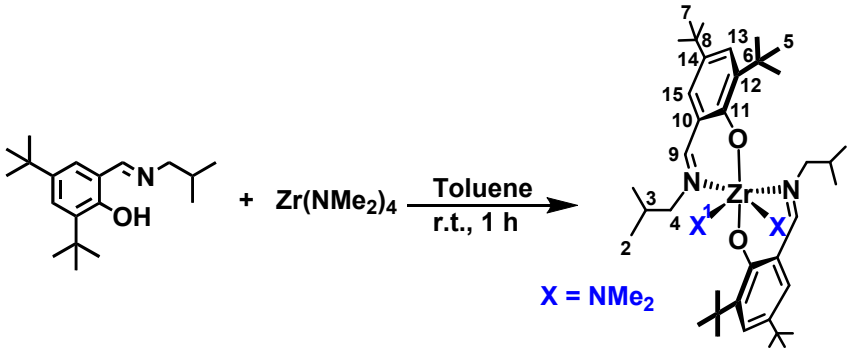

$Zr(NMe_2)_4$ (1.32 g, 4.94 mmol, 1.0 equiv) and **FI-H** ligand (3.00 g, 10.38 mmol, 2.1 equiv) were combined in toluene (30 mL) at rt. After 1 h, all volatiles were removed in vacuo, and the resulting solid was washed with pentane. The resulting yellow solid was then collected and dried under high vacuum. The filtrate was concentrated for further crystallization, and a second crop of product was then collected (3.14 g, 84% yield). Single crystals suitable for X-Ray diffraction studies were grown from a solution of toluene/*n*-hexane at rt. ^{1}H and ^{13}C NMR peaks were assigned through a combined analysis of ^{1}H NMR, ^{13}C NMR, ^{1}H, ^{1}H-gCOSY, gHSQCAD, and gHMBCAD spectroscopy. ^{1}H NMR (400 MHz, C_6D_6) δ 7.87 (s, 2H, H9), 7.79 (d, J = 2.6 Hz, 2H, H15), 7.22 (d, J = 2.5 Hz, 2H, H13), 3.51 (dd, J = 10.4, 4.0 Hz, 2H, H4), 3.23 (s, 12H, H1), 2.41 (t, J = 10.4 Hz, 2H, H4'), 1.95 (m, 2H, H3), 1.83 (s, 18H, H5), 1.32 (s, 18H, H7), 0.57 (t, J = 6.9 Hz, 12H, H2). ^{13}C NMR (101 MHz, C_6D_6) δ 168.04 (C9), 160.37, 139.76, 139.29, 129.66, 129.12, 122.63, 70.43 (C4), 45.33 (C1), 35.94, 34.30, 31.70, 30.13, 28.80 (C3), 21.49 (C2), 19.84 (C2'). Elem. Anal. Calcd for $C_{42}H_{72}N_4O_2Zr$: C 66.70, H 9.60, N 7.41; Found: C 66.82, H 9.76, N 7.26

3) Synthesis of the Complex FI_2ZrBn_2 (2)

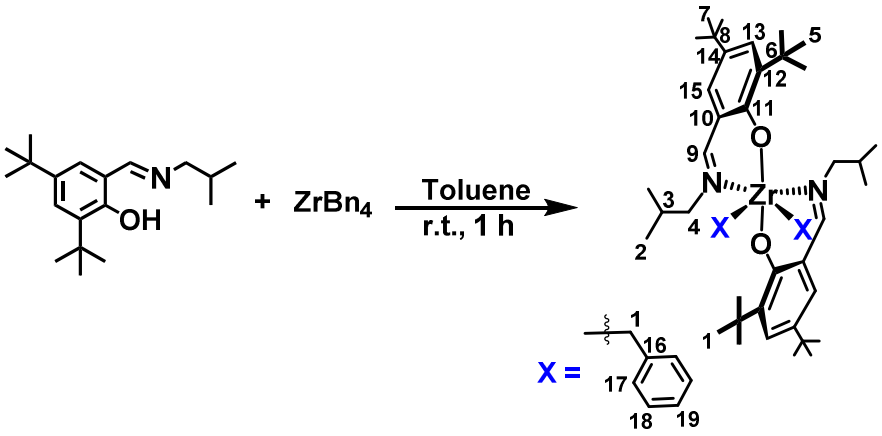

$ZrBn_4$ (0.46 g, 1.00 mmol, 1.0 equiv) and **FI-H** ligand (0.58 g, 2.00 mmol, 2.0 equiv) were combined in toluene (20 mL) at rt. After 1 h, all volatiles were removed in vacuo, and the resulting solid was dissolved in *n*-hexane for recrystallization. The product was collected as an orange solid and dried under high vacuum (0.51 g, 60% yield). ^{1}H and ^{13}C NMR peaks were assigned through a combined analysis of ^{1}H NMR, ^{13}C NMR, ^{1}H, ^{1}H-gCOSY, gHSQCAD, and gHMBCAD spectroscopy. ^{1}H NMR (600 MHz, C_6D_6) δ 7.73 (d, J = 2.5 Hz, 2H, H15), 7.58 (s, 2H, H9), 7.05 – 7.03 (m, 4H, H17), 7.01 (d, J = 2.6 Hz, 2H, H13), 6.92 (t, J = 7.7 Hz, 4H, H18), 6.73 – 6.70 (m, 2H, H19), 3.72 – 3.58 (m, 2H, H4), 2.80 (q, J = 9.7 Hz, 4H, H1), 2.52 (*m*, 2H, H4), 1.80 (s, 18H), 1.38 (m, 2H, H3), 1.29 (s, 18H), 0.37 (m, 12H, H2). ^{13}C NMR (151 MHz, C_6D_6) δ 168.73 (C9), 158.41, 146.51 (C16), 140.54, 138.24, 129.68, 129.20, 127.99 (C18), 127.28 (C17), 123.62, 120.38 (C19), 69.00 (C1), 64.91 (C4), 35.42, 33.93, 31.25, 30.25, 27.30 (C3), 19.92 (C2), 19.57 (C2'). Elem. Anal. Calcd for $C_{52}H_{74}N_2O_2Zr$: C, 73.44; H, 8.77; N, 3.29; Found: C 73.27, H 8.86, N 3.41

4) Synthesis of the Complex FI_2ZrMe_2 (3)

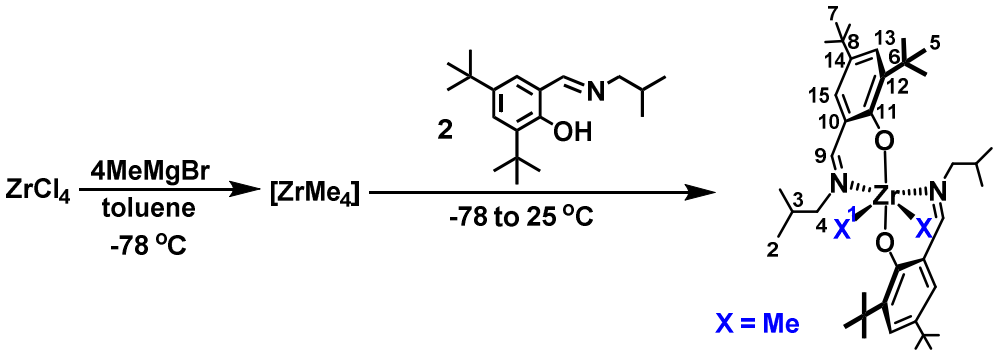

The complex was synthesized based on a modified literature procedure.[3] To a suspension of **$ZrCl_4$** (0.466 g, 2.0 mmol, 1.0 equiv) in anhydrous toluene (60 mL) in a Schlenk flask at −78 °C

was added dropwise a solution of **MeMgBr** in diethyl ether (3.0 M, 2.8 mL, 8.4 mmol, 4.2 equiv). The resulting mixture was stirred at −78 °C for an additional 30 min, and then a solution of **FI-H** ligand (1.156 g, 4.0 mmol, 2.0 equiv) in toluene (20 mL) was added slowly at −78 °C. The resulting suspension was allowed to stir at −78 °C for 2 h, and then the reaction mixture was allowed to warm to rt by removal of the cooling bath, to give a pale yellow mixture. After stirring at rt for an additional 1 h, all volatiles were removed under reduced pressure, and the residue was then extracted with toluene. Toluene was then removed under high vacuum to give a mixture, to which pentane was added. The precipitate was collected by filtration and dried under high vacuum to yield the product as a light yellow solid (0.89 g, 63% yield). ^{1}H NMR (600 MHz, C_7D_8/DFB = 10/1, v/v, 25 ºC) δ 7.83 (s, 2H, H9), 7.75 (d, *J* = 2.5 Hz, 2H), 7.12 (d, *J* = 2.5 Hz, 2H), 2.13 – 2.09 (m, 2H), 1.80 (s, 18H), 1.30 (s, 18H,), 0.63 (s, 6H, H1), 0.50 (d, *J* = 6.6 Hz, 12H, H2). ^{13}C NMR (151 MHz, C_7D_8/DFB = 10/1, v/v, 25 ºC) δ 168.98 (C9), 159.44, 140.76, 139.70, 130.27, 129.27, 122.92, 69.92 (C4), 40.67 (C1), 35.87, 34.41, 31.61, 30.11, 28.33 (C3), 20.00 (C2, confirmed by HSQC). Elem. Anal. Calcd for $C_{40}H_{66}N_2O_2Zr$: C 68.81, H 9.53, N 4.01; Found: C 68.68, H 9.37, N 4.04

Due to significant broadening at 25 ºC, the resonances corresponding to the C=N-$\underline{CH_2}CH(CH_3)_2$ protons are not obervable in the ^{1}H NMR spectrum at this temperature. The stereochemically nonrigid coordination geometry of the two FI ligands[4-7] is the likely reason for the broadening of the C=N-$\underline{CH_2}CH(CH_3)_2$ peaks. The ^{1}H NMR of C=N-$CH_2\underline{CH}(CH_3)_2$, which is one carbon further from the imine, is not influenced. VT NMR spectroscopy was used to identify these peaks (**Figure S9**) in the temperature range 25 to -50 ºC. The complex is unstable at temperatures above 25 ºC and undergoes significant decomposition during NMR data collection.

5) Synthesis of the Complex FI_2ZrCl_2 (4)

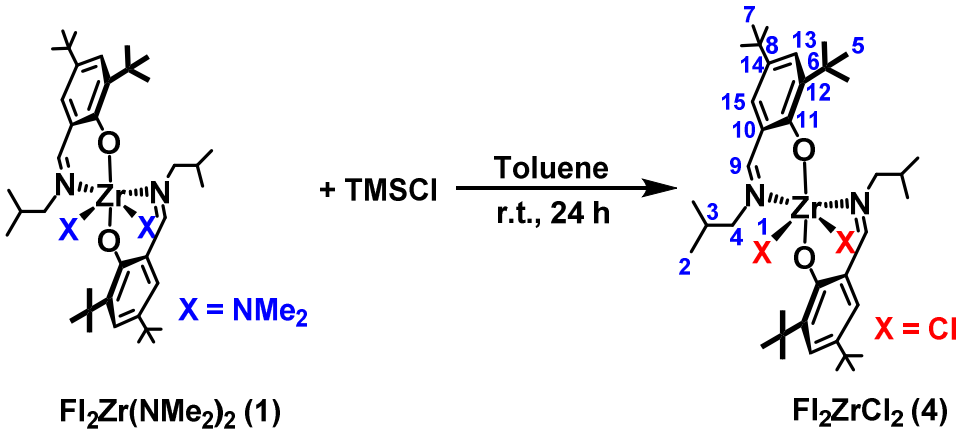

$FI_2Zr(NMe_2)_2$ (1) (1.04 g, 1.4 mmol, 1.0 equiv) was dissolved in toluene (40 mL) in a 100-mL reaction flask. TMSCl (3.5 mL, 27.6 mmol, 19.7 equiv) was added via syringe at 25 ºC. The solution was then stirred at rt for 24 h. All volatiles were then removed under reduced pressure and the resulting residue was washed with *n*-hexane. The resulting solid was dried under high vacuum and the product was collected as a yellow solid (0.73 g, 69% yield). Single crystals suitable for X-ray diffraction studies were grown from a solution of toluene at –40 ºC. Complexes with similar structures were reported by Fujita et al.[8] exhibiting complicated patterns in the ^{1}H NMR spectrum, likely due to the presence of isomers. The ^{1}H and ^{13}C peaks were assigned through a combined analysis of ^{1}H NMR, ^{13}C NMR, ^{1}H, ^{1}H-gCOSY, gHSQCAD, and gHMBCAD spectroscopy. ^{1}H NMR (600 MHz, C_6D_5Cl) δ 7.98 (s, 2H, H9), 7.75 (d, J = 2.5 Hz, 2H, H13), 7.23 (d, J = 2.5 Hz, 2H, H15), 3.44 (dd, J = 11.5, 5.7 Hz, 2H, H4), 2.99 (dd, J = 11.5, 9.0 Hz, 2H, H4'), 2.25 (m, 2H, H3), 1.70 (s, 18H), 1.27 (s, 18H, H5), 0.55 (m, 12H, H2); ^{13}C NMR (151 MHz, C_6D_5Cl) δ 170.02 (C9), 157.92, 142.44, 139.40, 131.80, 129.09, 122.71, 69.84 (C4), 35.49, 34.28, 31.30, 30.02, 28.16 (C3), 20.39 (C2), 19.20 (C2'); Elem. Anal. Calcd for $C_{38}H_{60}Cl_2N_2O_2Zr$: C, 61.76; H, 8.18; N, 3.79; Found: C 61.58, H 8.08, N 3.64

6) Synthesis of the Complex $FIAlMe_2$, Al (5)

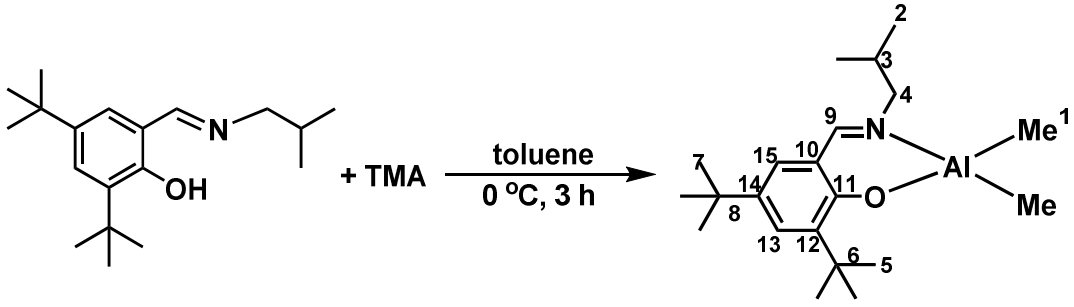

This complex was synthesized based on a modified literature procedure:[9] **FI-H** (0.63 g, 2.2 mmol) was dissolved in toluene (10 mL) in a 100-mL reaction flask. **TMA** (2.0 M in toluene) was added via syringe at 0 ºC. The solution was then stirred at 0 ºC for 1 h. All volatiles were then removed under reduced pressure and the resulting residue was recrystallized from pentane. The resulting solid was dried under high vacuum and the product was collected as a solid (0.34 g, 45% yield). Single crystals were obtained by cooling a pentane solution in freezer. ^{1}H NMR (600 MHz, C_6D_6) δ 7.79 (d, *J* = 2.6 Hz, 1H, H13), 7.39 (s, 1H, H9)), 6.93 (d, *J* = 2.6 Hz, 1H, H15), 2.93 (d, *J* = 7.6 Hz, 2H), 2.07 – 1.99 (m, 1H, H3), 1.71 (s, 9H, H5), 1.42 (s, 9H, H7), 0.67 (d, *J* = 6.7 Hz, 6H, H2), -0.14 (s, 6H, H1). ^{13}C NMR (151 MHz, C_6D_6) δ 171.89 (C9), 162.12, 140.98, 138.95, 131.73 (C13), 128.86 (C15), 118.83, 66.04 (C4), 35.64 (C6), 34.17 (C8), 31.57 (C7), 29.65 (C5), 28.31 (C3), 19.92 (C2), -9.11 (C1, very weak signal and confirmed by HSQC experiment); Elem. Anal. Calcd for $C_{21}H_{36}AlNO$: C 73.00, H 10.50, N 4.05; Found: C 73.13, H 10.67, N 4.06

7) Synthesis of the Complex FIZr(NMe$_2$)$_3$ (6)

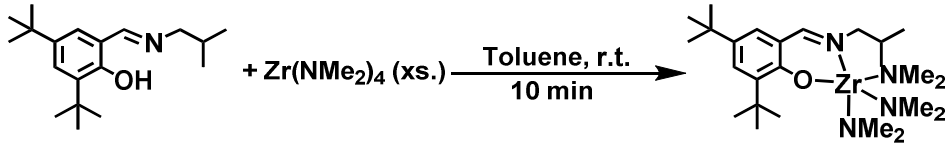

Zr(NMe$_2$)$_4$ (6.77 g, 25.3 mmol, 3.1 equiv) was dissolved in toluene (20 mL) in a Schlenk flask. A solution of **FI-H** ligand (2.35 g, 8.13 mmol, 1.0 equiv) in toluene (30 mL) was then added slowly at rt over the course of 10 min. All volatiles were then removed under reduced pressure. Excess **Zr(NMe$_2$)$_4$** was removed by sublimation at 60 ºC under high vacuum. The remaining crude product was purified by crystallization from a solution of pentane, dried under high vacuum, and the product was isolated as a yellow solid (3.4 g, 82% yield). Single crystals suitable for X-Ray diffraction studies were grown from slow evaporation of a pentane solution at rt. ^{1}H NMR (400 MHz, C_6D_6) δ 7.90 (s, 1H), 7.72 (d, *J* = 2.5 Hz, 1H), 7.16 (d, *J* = 2.4 Hz, 1H), 3.16 (d, *J* = 7.1 Hz, 2H), 3.08 (s, 18H), 1.83 (m, 1H), 1.66 (s, 9H), 1.36 (s, 9H), 0.72 (d, *J* = 6.7 Hz, 6H). ^{13}C NMR (101 MHz, C_6D_6) δ 169.33, 160.78, 139.97, 139.74, 129.45, 128.93, 121.71, 70.36, 42.85, 35.67, 34.33, 31.76, 29.75, 28.30, 20.76. Elem. Anal. Calcd for $C_{25}H_{48}N_4OZr$: C 58.66, H 9.45, N 10.94; Found: C 58.43, H 9.32, N 10.74

8) Synthesis of the Complex Al$_2$(NMe$_2$)$_2$Me$_4$

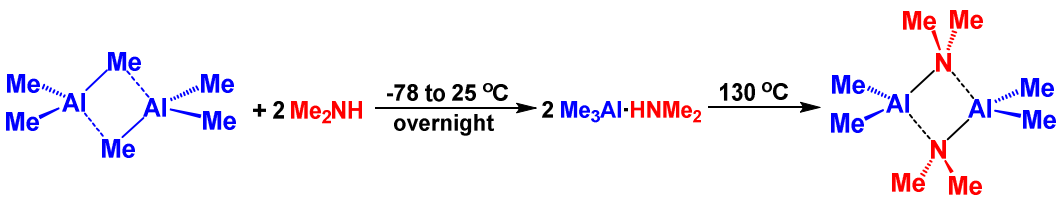

This complex was synthesized based on a modified literature procedure.[10] To **Me_2NH** (10 mmol, 2.0 M in THF, 5mL) in a Schlenk flask at −78 °C was added dropwise **trimethylaluminum** (**TMA**, 10 mmol, 2.0 M in toluene, 5 mL). The resulting mixture was stirred at −78 °C for an additional 30 min, and then let it warm to 25 °C for overnight reaction. All volatiles were removed under high vacuum to give white powder, ^{1}H NMR confirms the structure of $Me_3Al{\cdot}HNMe_2$. ^{1}H NMR (499 MHz, C_6D_6) δ 1.51 (m, 6H), 0.68 (br, 1H), 0.57 (s, 9H). Under argon, the white powder was put in a schlenk flask and heated at 130 °C until no gas evolution (CH_4, about 1 h). The resulting white needle-like product was also sublimed inside the top of the Schlenk flask which is the desired product $Al_2(NMe_2)_2Me_4$, 0.73 g, 73% yield. ^{1}H NMR confirms the structure.[10] ^{1}H NMR (600 MHz, C_6D_6) δ 2.06 (s, 12H), 0.57 (s, 12H).

Polymerization Experiments (Table 1 in the manuscript)

Preparation of catalyst solutions. Catalyst solutions were prepared immediately prior to use. The procedures for preparing catalyst solutions: In a glovebox, 10 μmol of catalyst was dissolved in 8 mL of toluene in a Schlenk flask. The Schlenk flask was then removed from the glovebox, connected to a Schlenk line, and the appropriate amount of TMA was added via syringe under argon. The catalyst solution was next stirred for 30 min and then 12 μmol of cocatalyst BT (6.0 mM in toluene, 2 mL) was added via syringe. The solution was stirred for 1 min before injecting into the reactor to initate polymerization.

Ethylene/1-octene copolymerization procedure. In a typical experiment, a 350-mL oven dried glass pressure vessel (350 mL, CG1880-42, Chemglass) equipped with a large stir bar was charged with dry toluene (45 mL) and 1-octene (3.58 g) inside a glovebox. The pressure vessel was sealed, removed from the glovebox, and attached to a high-pressure/high-vacuum line. The mixture was cooled to –78 °C in a dry ice/acetone bath, degassed, filled with ethylene gas, sealed, and then allowed to warm to the required temperature with an external bath. A solution of catalyst/cocatalyst was quickly injected into the flask with rapid stirring using a gas-tight syringe equipped with a flattened spraying needle under argon. The reactor was pressurized with the

required pressure of ethylene. After the required reaction time, the polymerization was quenched with methanol. The reactor was then vented, and the polymerization mixture was quenched with 10% HCl in methanol. The precipitated polymer was stirred for several hours, collected by filtration, and washed with methanol. It was then dried under high vacuum at 80 °C overnight until a constant weight was obtained.

Polymerization Experiments (Table 2 in the manuscript)

Ethylene-1-octene copolymerization. A 2-liter Parr reactor was used in the polymerizations. All feeds were passed through columns of alumina and Q-5™ catalyst (available from Engelhard Chemicals Inc.) prior to introduction into the reactor.[1] The stirred 2-liter reactor was charged with about 609 g of mixed alkanes solvent (Isopar E) and 300 g of 1-octene comonomer. The reactor contents were heated to the polymerization temperature of 120 °C. Once at temperature, the reactor was saturated with ethylene at 270 psig. Precatalysts and trityl borate activator, as 5 mM and 6 mM solutions in toluene, respectively, were mixed in a glovebox at room temperature and transferred directly to a catalyst addition tank through stainless steel tubing and injected into the reactor with a nitrogen overpressure. In some polymerizations the precatalyst was mixed with trimethylaluminum for either less than two min or for at least 30 min before trityl borate was added and the activated solution was added to the reactor. The polymerization conditions were maintained for up to 10 min with ethylene added on demand. Heat was continuously removed from the reaction vessel through an internal cooling coil. The resulting solution was removed from the reactor, quenched with isopropyl alcohol, and stabilized by addition of 10 mL of a toluene solution containing approximately 67 mg of a hindered phenol antioxidant (Irganox™ 1010 from Ciba Geigy Corporation) and 133 mg of a phosphorus stabilizer (Irgafos™ 168 from Ciba Geigy Corporation). Between polymerization runs, a wash cycle was conducted in which 850 g of mixed alkanes (Isopar E) were added to the reactor and the reactor was heated to 150 °C. The reactor was then emptied of the heated solvent immediately before beginning a new polymerization run. Polymers were recovered by drying for about 12 h in a temperature-ramped vacuum oven with a final set point of 140 °C.

NMR Spectra of the Ligand and Complexes

1) **FI-H Ligand**

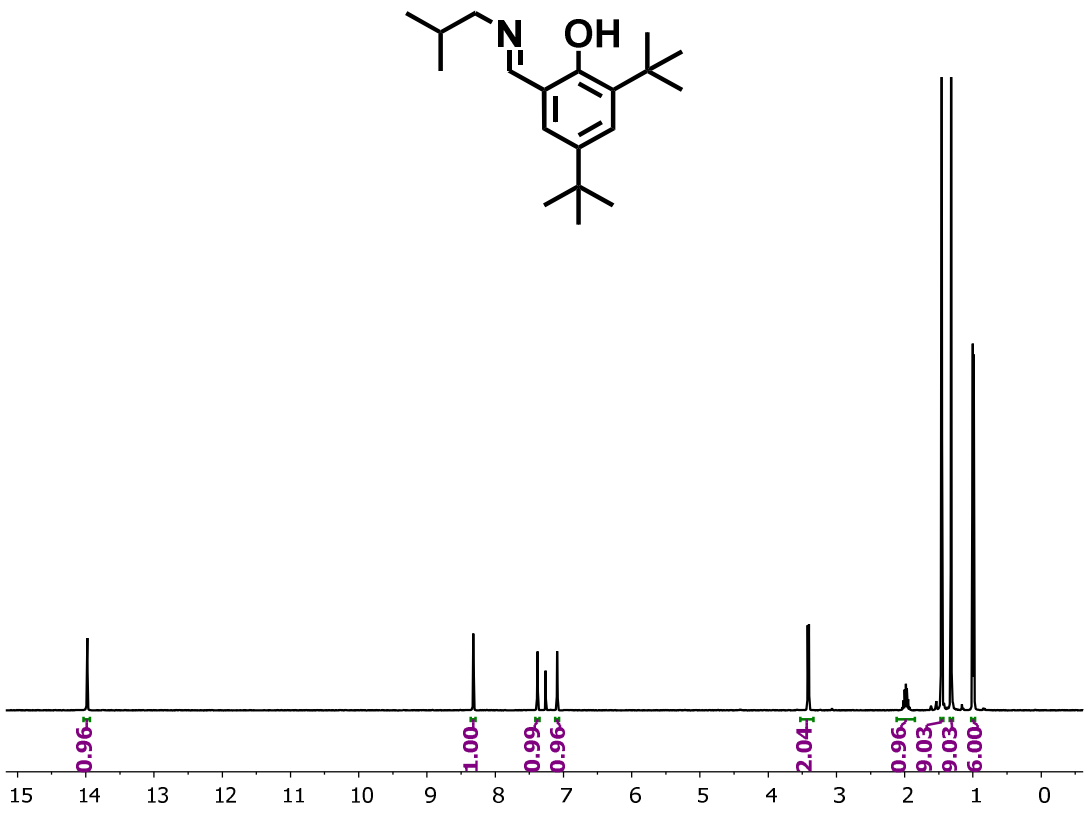

Figure S1. ^{1}H NMR spectrum (400 MHz) of **Ligand FI-H** in $CDCl_3$.

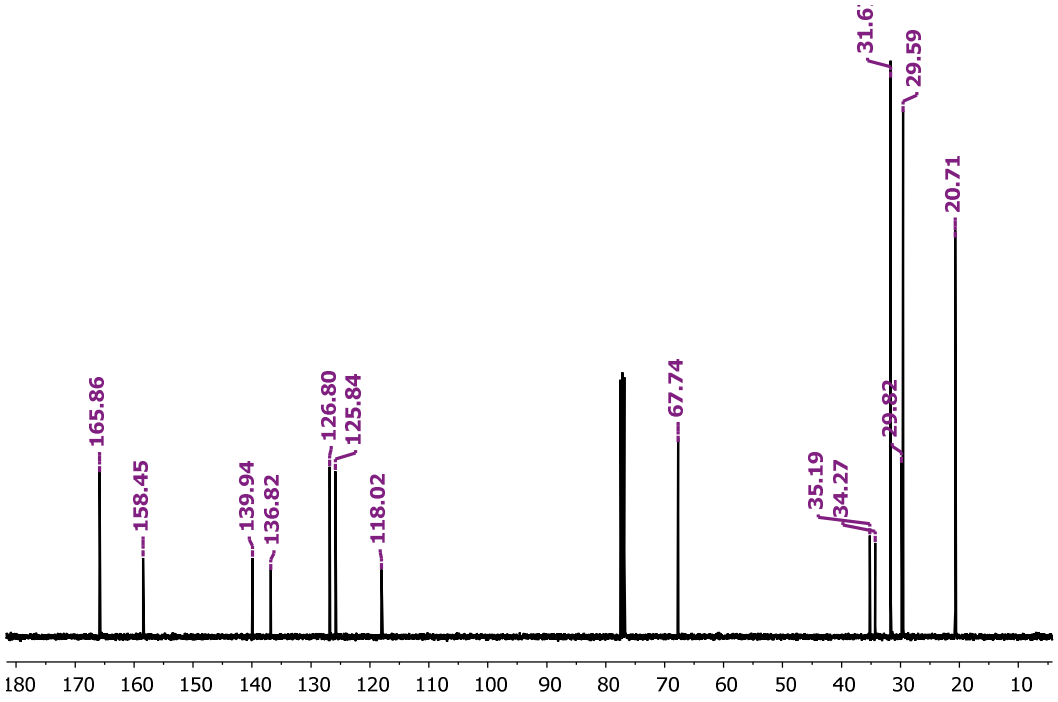

Figure S2. ^{13}C NMR spectrum (101 MHz) of **Ligand FI-H** in $CDCl_3$.

2) Complex $FI_2Zr(NMe_2)_2$ (1)

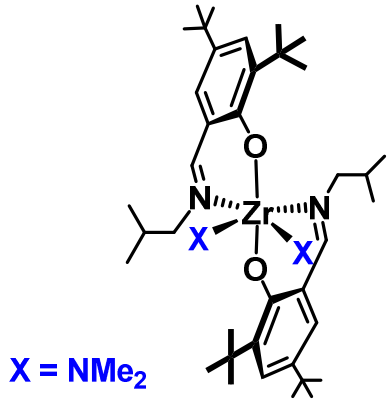

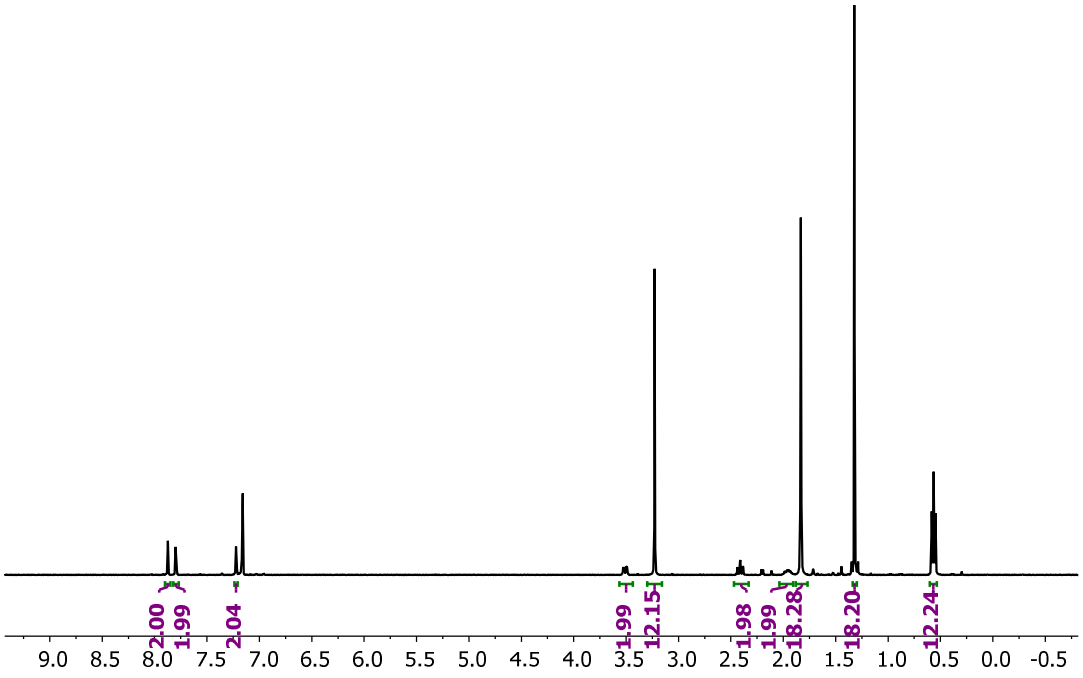

Figure S3. ^{1}H NMR spectrum (400 MHz) of complex **$FI_2Zr(NMe_2)_2$ (1)** (C_6D_6, 25 ºC).

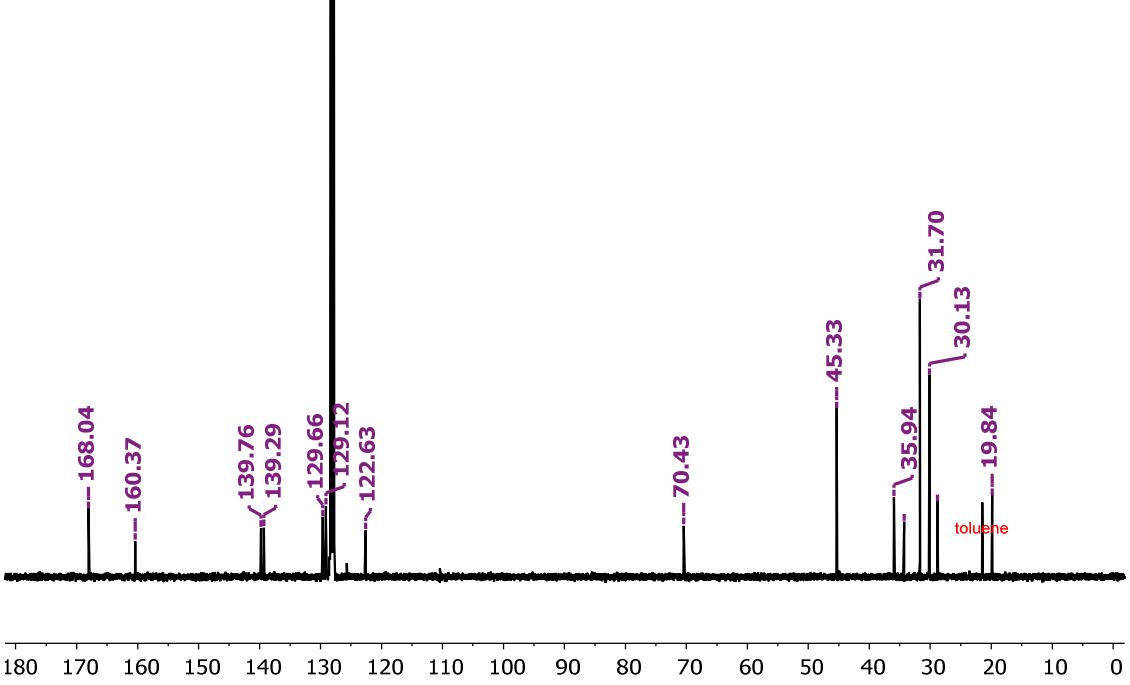

Figure S4. ^{13}C NMR spectrum (101 MHz) of complex **$FI_2Zr(NMe_2)_2$ (1)** (C_6D_6, 25 ºC).

3) Complex FI_2ZrBn_2 (2)

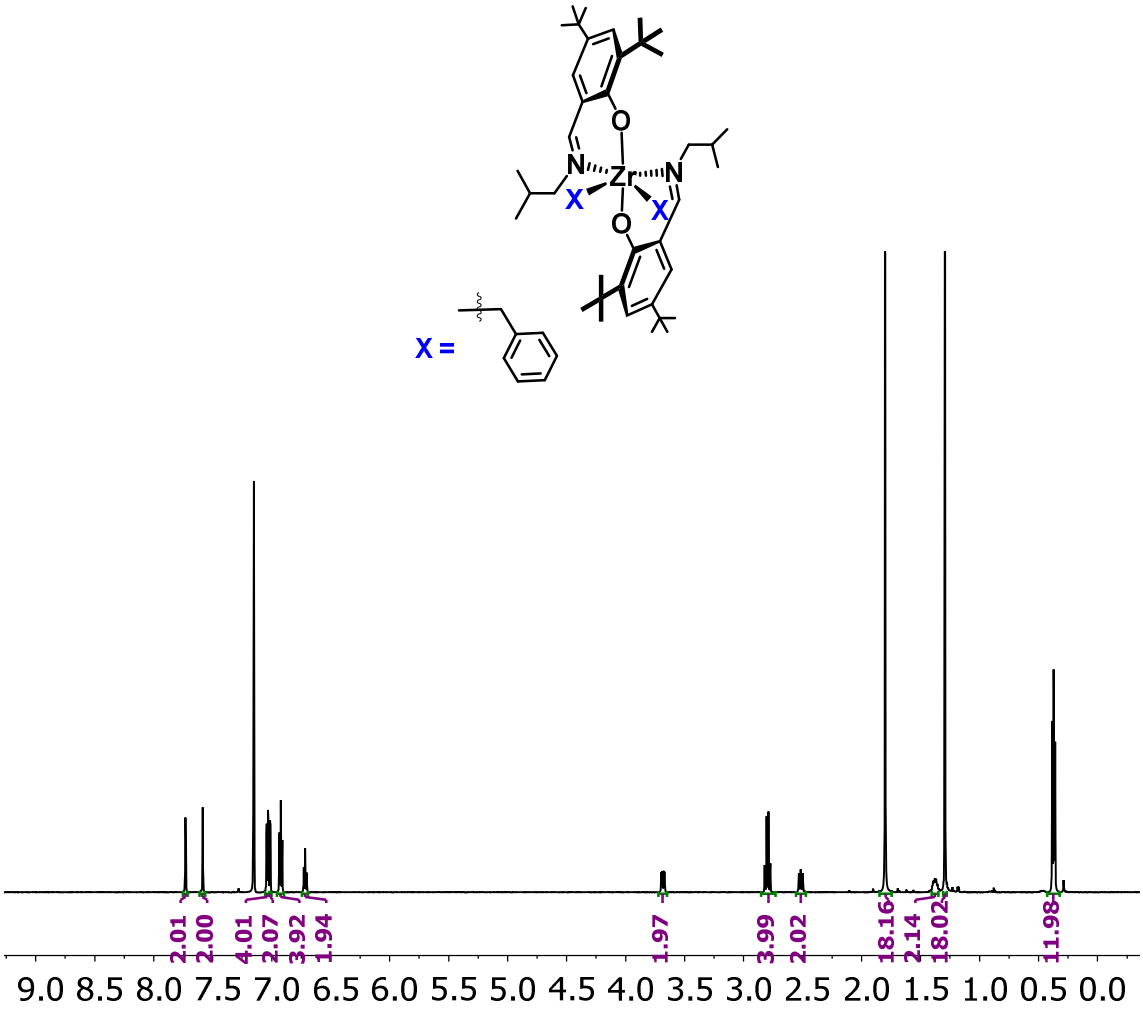

Figure S5. ^{1}H NMR spectrum (600 MHz) of complex **FI_2ZrBn_2 (2)** (C_6D_6, 25 ºC).

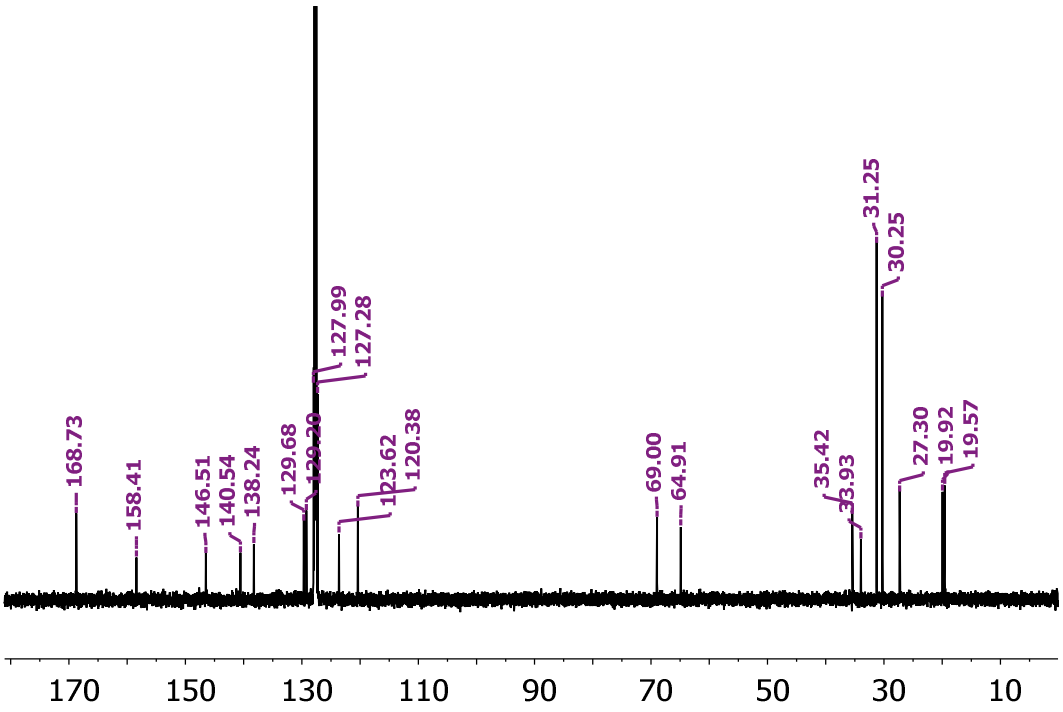

Figure S6. ^{13}C NMR spectrum (151 MHz) of complex **FI$_2$ZrBn$_2$ (2)** (C_6D_6, 25 °C).

4) Complex FI$_2$ZrMe$_2$ (3)

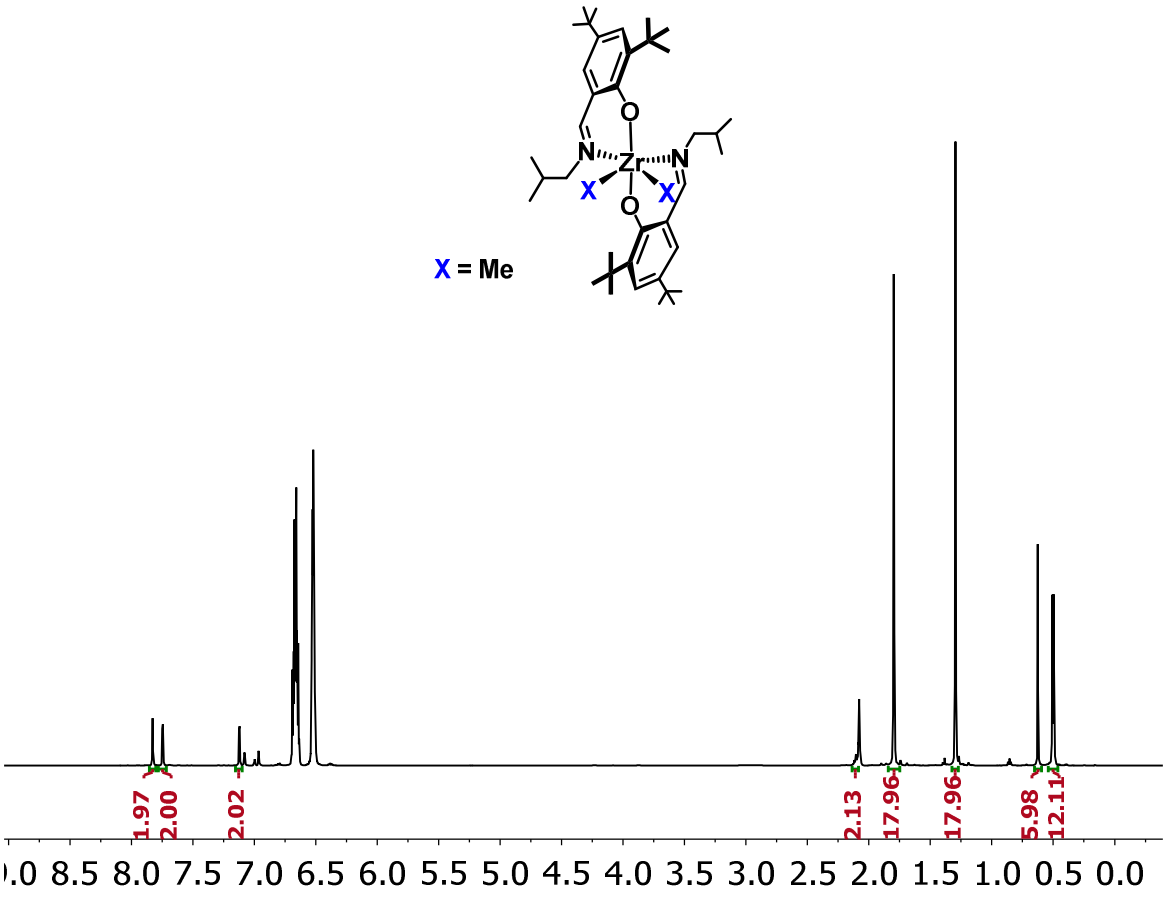

Figure S7. ^{1}H NMR spectrum (600 MHz) of complex **FI$_2$ZrMe$_2$ (3)** (C_7D_8/DFB = 10/1, *v/v*, 25 °C)

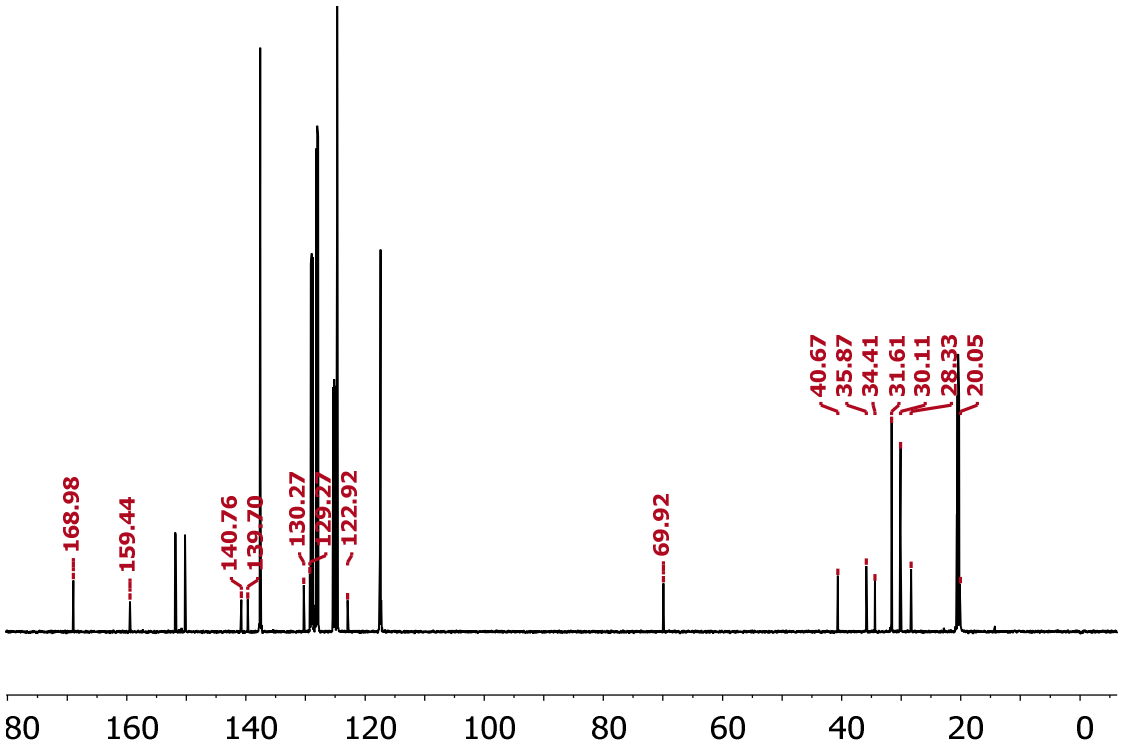

Figure S8. ^{13}C NMR spectrum (151 MHz) of complex **FI$_2$ZrMe$_2$ (3)** (C_7D_8/DFB = 10/1, *v/v*, 25 °C)

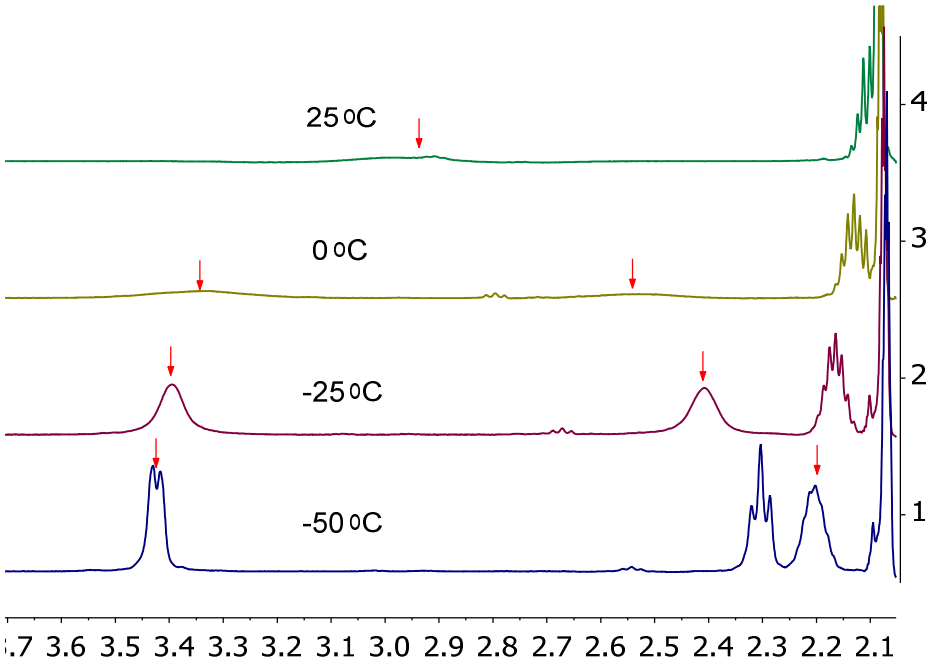

Figure S9. A section of VT ^{1}H NMR spectrum(600 MHz) of complex **FI$_2$ZrMe$_2$ (3)** (C_7D_8/DFB = 10/1, *v/v*)

5) Complex FI_2ZrCl_2 (4)

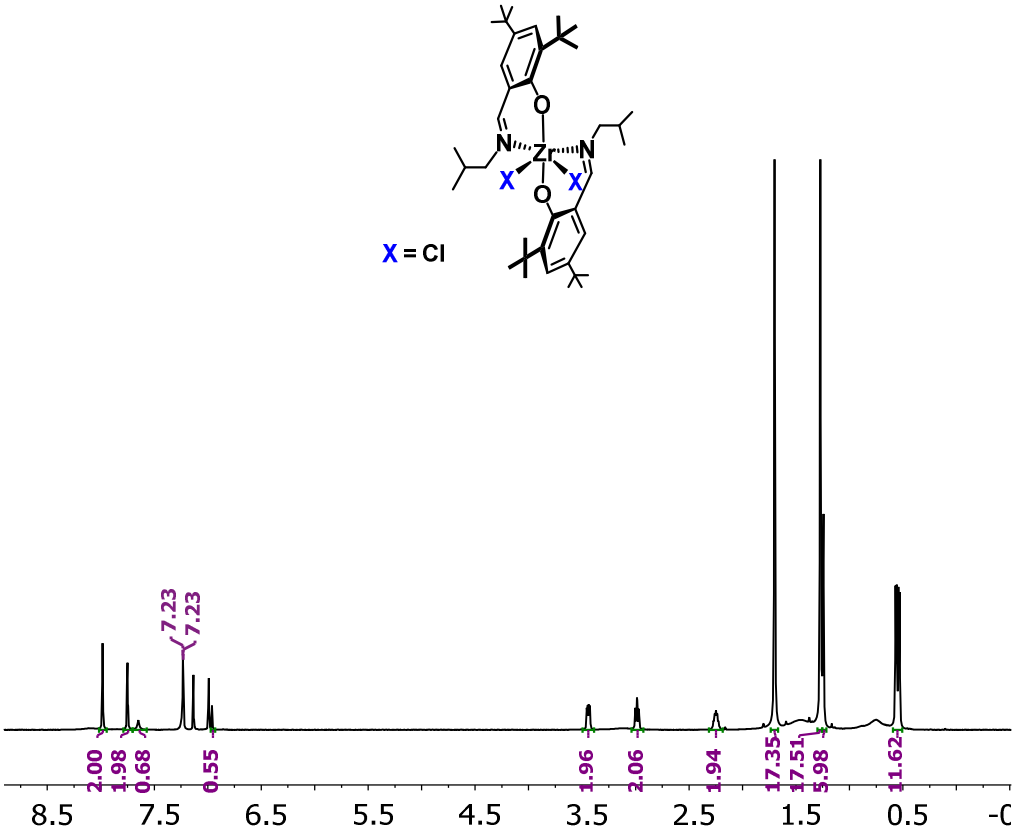

Figure S10. ^{1}H NMR spectrum (600 MHz) of **FI_2ZrCl_2 (4)** ($CDCl_3$, 25 ºC).

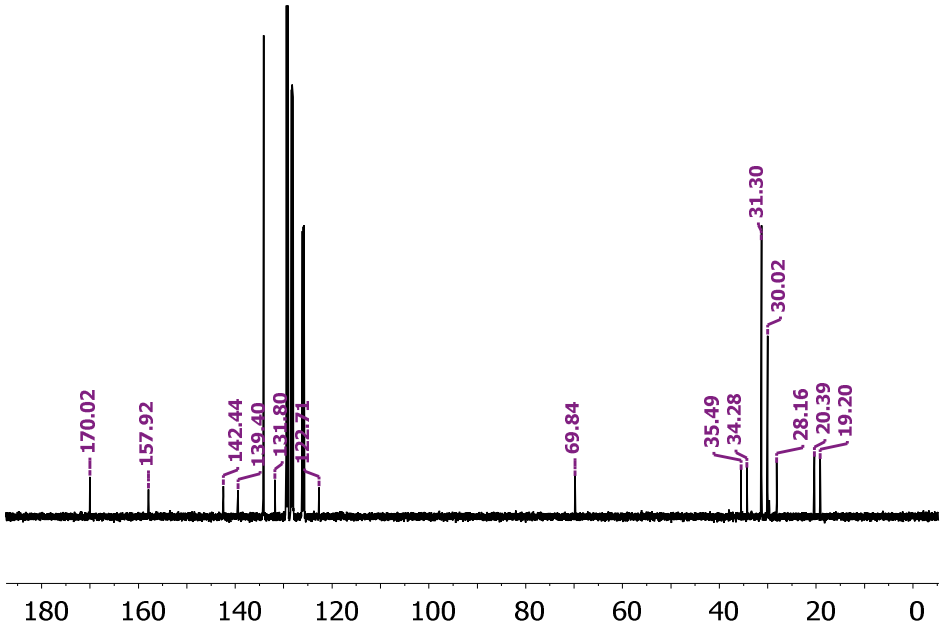

Figure S11. ^{13}C NMR spectrum (151 MHz) of **FI_2ZrCl_2 (4)** ($CDCl_3$, 25 ºC).

6) Complex FIAlMe$_2$ (5)

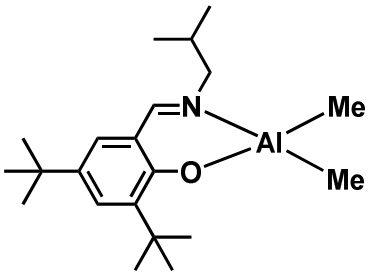

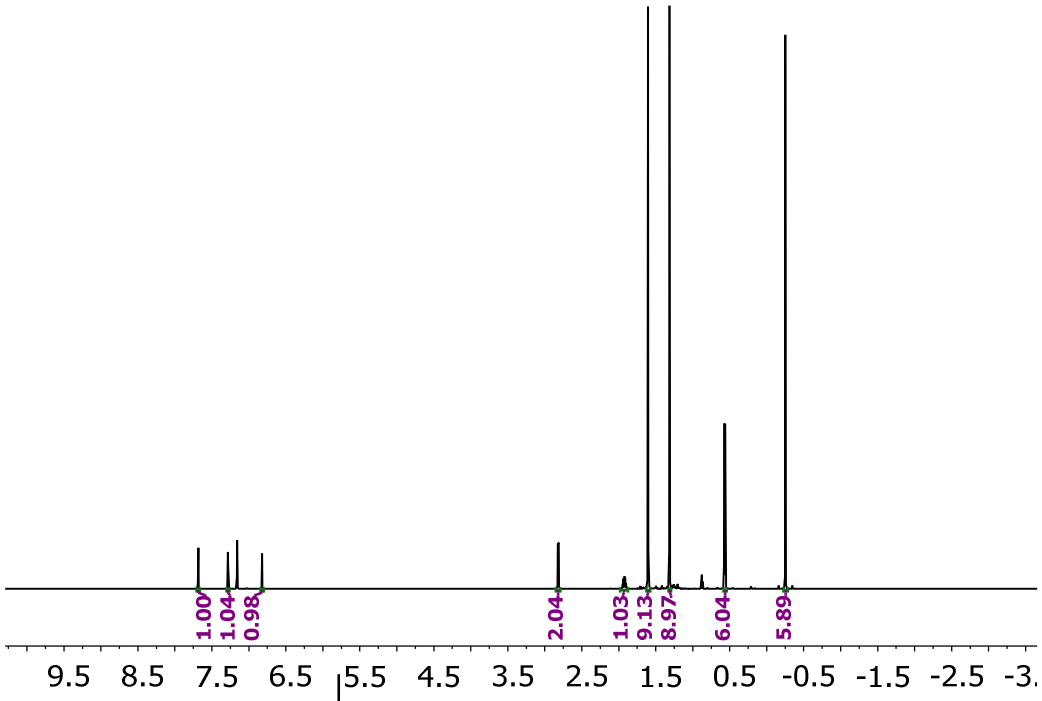

Figure S12. ^{1}H NMR spectrum (600 MHz) of complex **FIAlMe$_2$ (5)** (C_6D_6, 25 ºC)

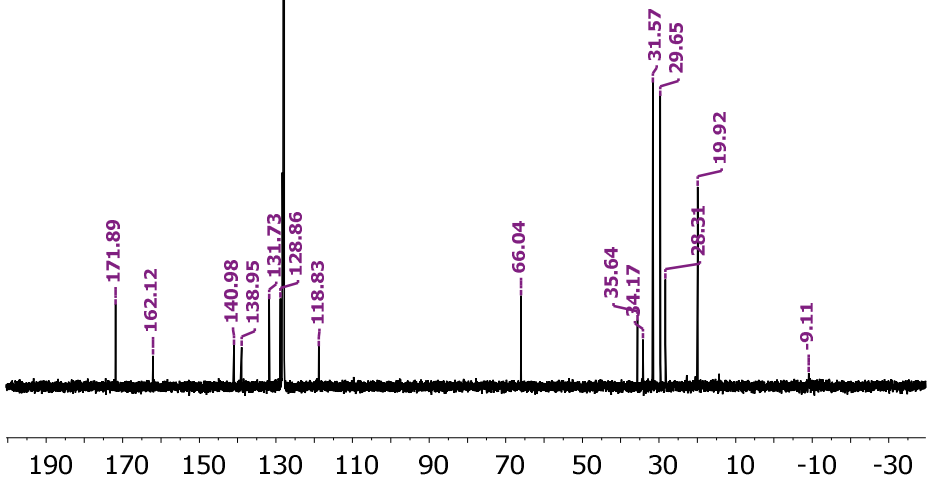

Figure S13. ^{13}C NMR spectrum (151 MHz) of complex **FIAlMe$_2$ (5)** (C_6D_6, 25 ºC)

7) Complex FIZr(NMe$_2$)$_3$ (6)

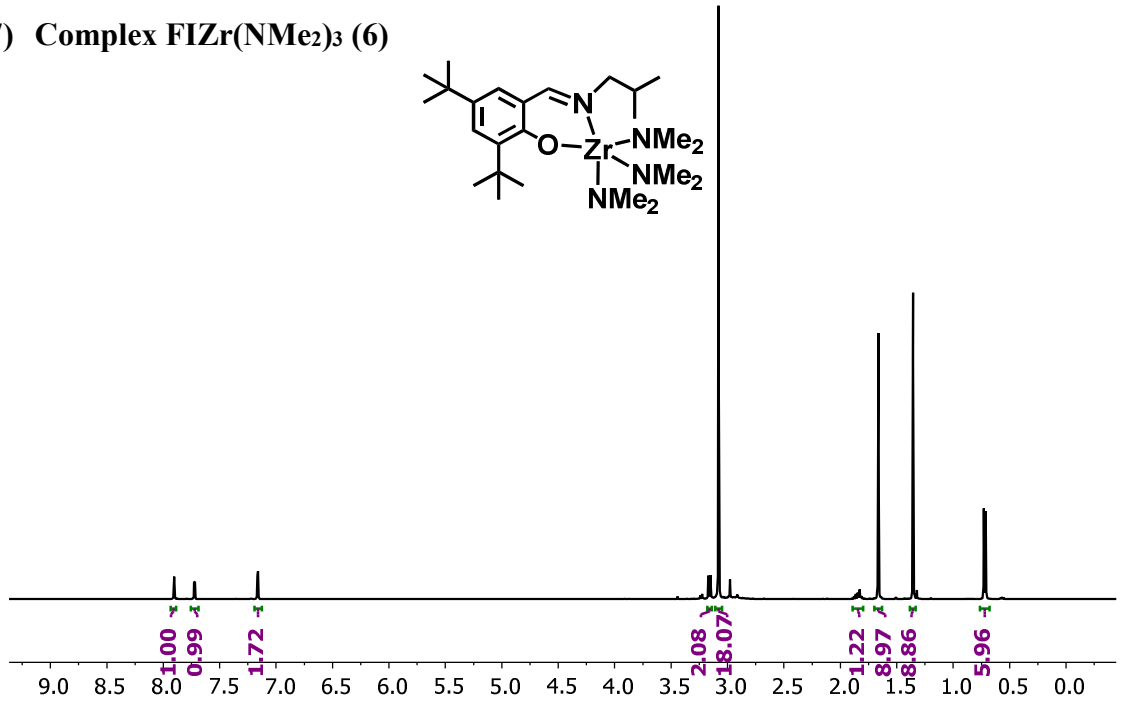

Figure S14. ^{1}H NMR spectrum (400 MHz) complex **FIZr(NMe$_2$)$_3$ (6)** (C_6D_6, 25 °C)

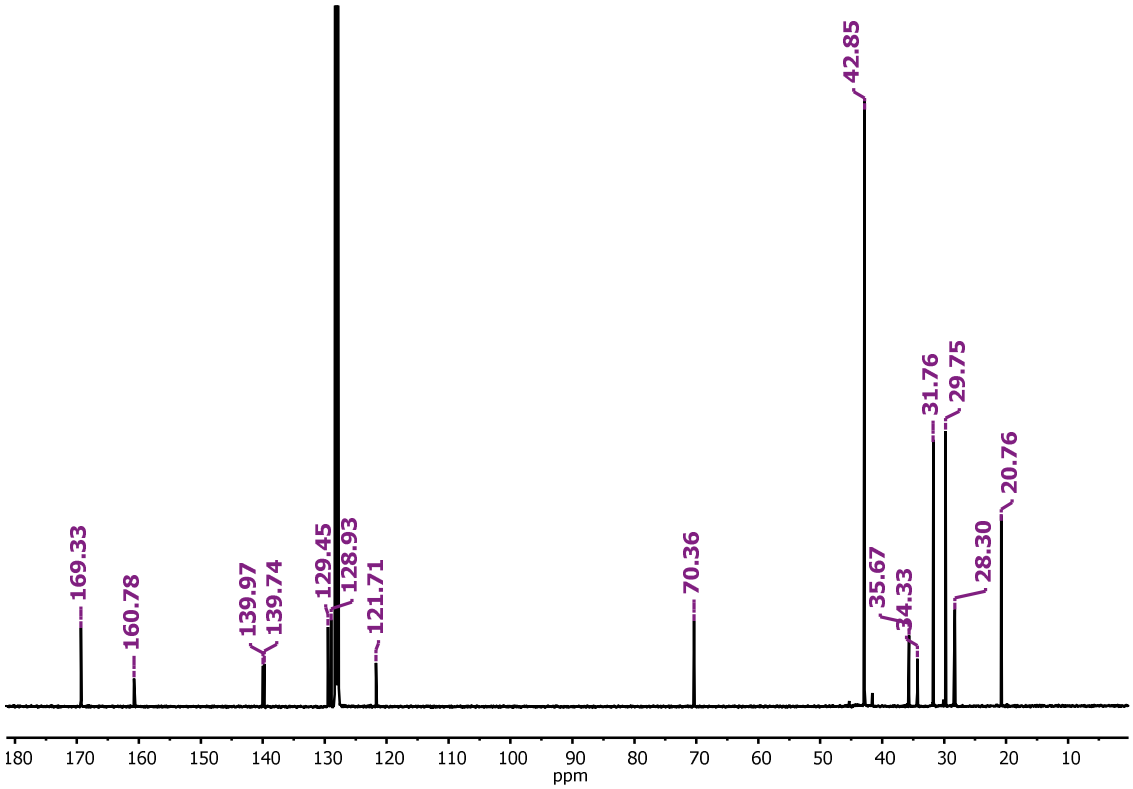

Figure S15. ^{13}C NMR spectrum (101 MHz) of complex **FIZr(NMe$_2$)$_3$ (6)** (C_6D_6, 25 °C)

8) Complex Me$_3$Al·HNMe$_2$

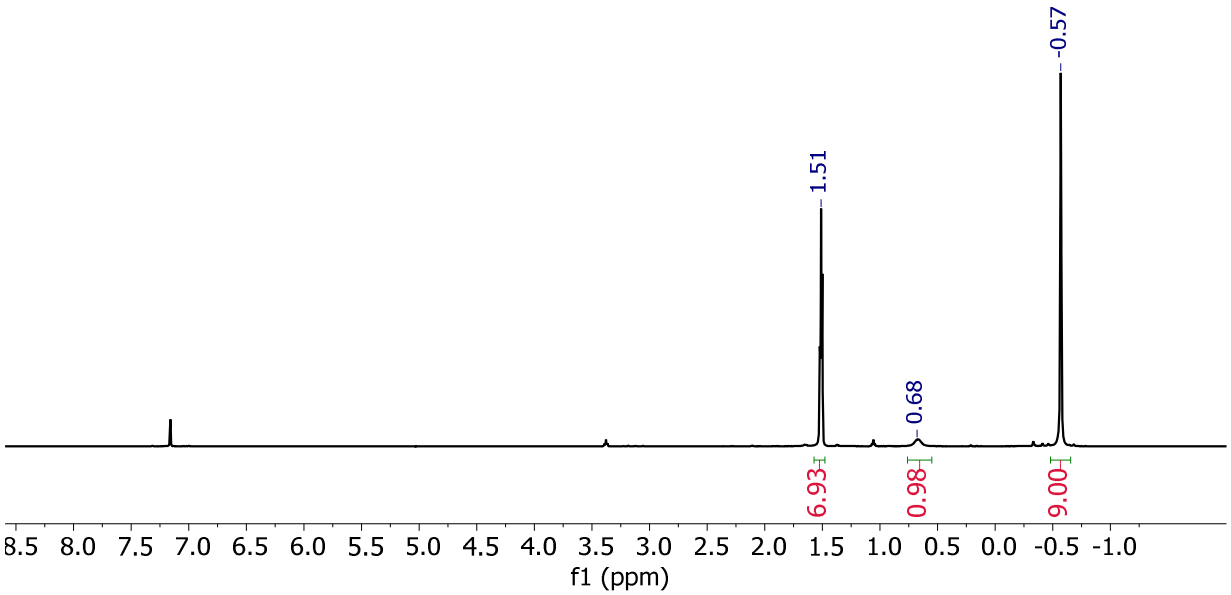

Figure S16. ^{1}H NMR spectrum (499 MHz) complex **$Me_3Al{\cdot}HNMe_2$** (C_6D_6, 25 °C)

9) Complex $Al_2(NMe_2)_2Me_4$

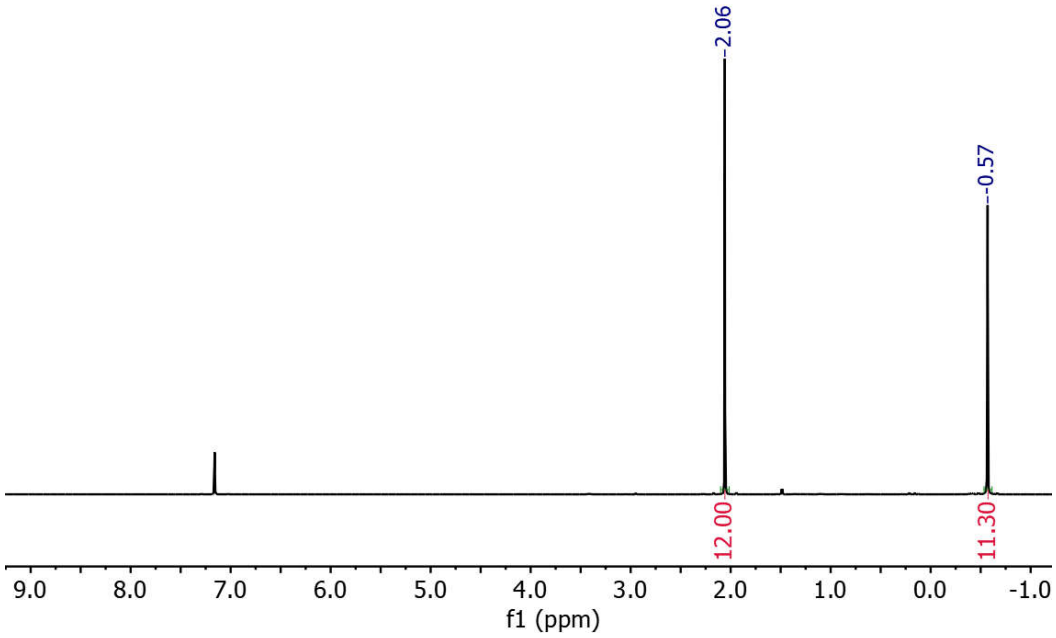

Figure S17. ^{1}H NMR spectrum (600 MHz) complex **$Al_2(NMe_2)_2Me_4$** (C_6D_6, 25 °C)

NMR Studies of Precatalyst Activation Chemistry

To better understand the precatalyst alkylation/activation process, the following experiments were carried out and their NMR spectra were analyzed.

1) Reaction of FI_2ZrMe_2 (3) + BT

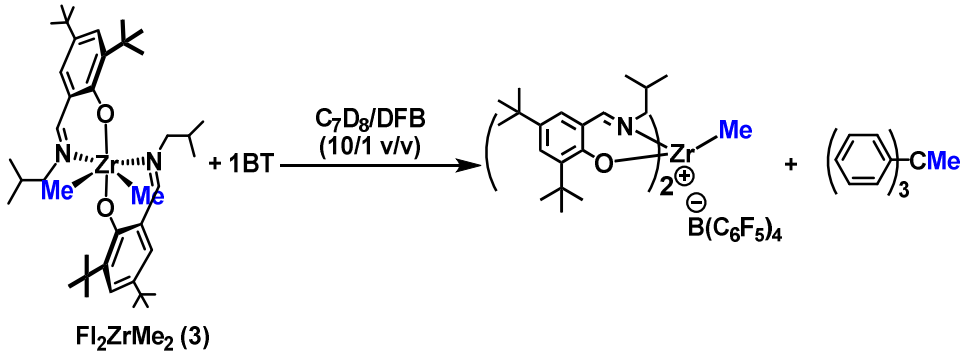

Procedure: In a glovebox, **FI_2ZrMe_2 (3)** (14.0 mg, 20 μmol, 1.0 equiv), BT (18.4 mg, 20 μmol 1.0 equiv), C_7D_8 (0.472 g, 0.5 mL) and DFB (0.058 g, 0.05 mL) were added to a vial. The vial was capped and the mixture was shaken for 1 min, the solution was then transferred into an NMR tube equipped with Precision Seal® rubber septum cap, and removed from the glovebox immediately in order to perform NMR experiments.

This reaction affords the cationic species **$FI_2ZrMe^+B(C_6F_5)_4^-$** quantitatively, as confirmed by NMR spectroscopy (**Figure S18**). ^{1}H NMR of **$FI_2ZrMe^+B(C_6F_5)_4^-$** (600 MHz, C_7D_8/DFB = 10/1, *v/v*, 25 ºC) δ 8.01 (s, 2H), 7.80 (d, J = 2.5 Hz, 2H), 7.25 (d, J = 2.5 Hz, 2H), 3.63 (s, 4H), 1.66 (m, 2H), 1.43 (s, 18H), 1.25 (s, 18H), 1.10 (s, 3H, Zr-*Me*, confirmed by HSQC), 0.68 (d, J = 6.6 Hz, 12H).

After standing at 25 ºC for 3 h, approx 32% decomposition was observed. In the calculation, Ph_3C-*Me* is used as an internal reference (peak **A**), peak **B** for C=NCH_2CH(*CH_3)$_2$* is used to represent the cationic species (**Figure S19**).

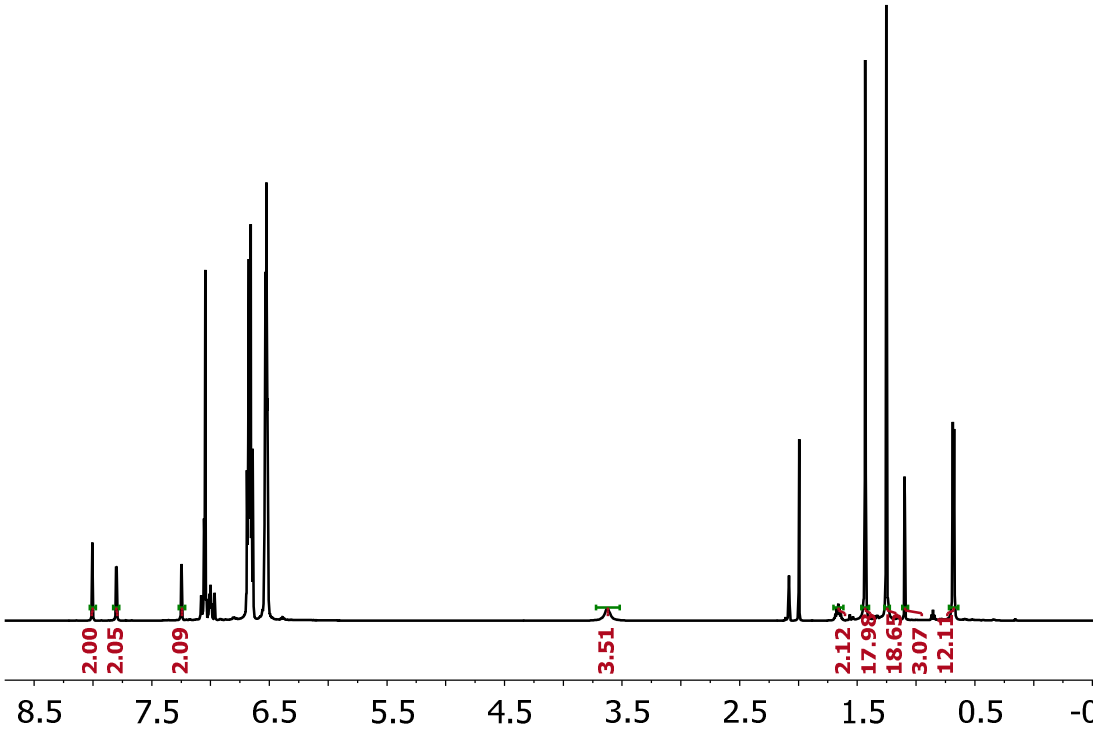

Figure S18. ^{1}H NMR spectrum (600 MHz) of cationic species, **$FI_2ZrMe^+B(C_6F_5)_4^-$** (C_7D_8/DFB = 10/1, *v/v*, 25 °C).

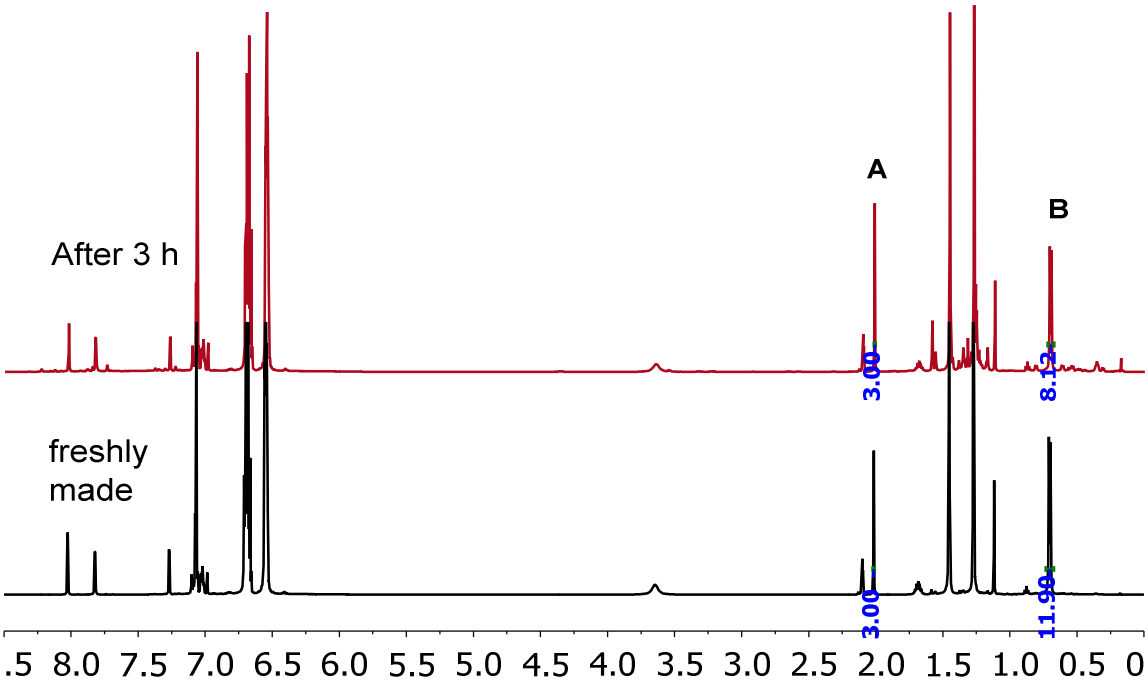

Figure S19. Decomposition over time. Comparison of ^{1}H NMR spectra of cationic species, **$FI_2ZrMe^+B(C_6F_5)_4^-$** (C_7D_8/DFB = 10/1, *v/v*, 25 °C), freshly made vs. after 3 h at rt. Peak **A** for

Ph_3C-*Me* is used as an internal reference, peak **B** for C=NCH_2CH(*CH_3*)$_2$ is used to represent the cationic species, **$FI_2ZrMe^+B(C_6F_5)_4^-$**.

2) Reaction of FI_2ZrMe_2 (3) + BT + TMA to give $FI_2Zr^+(\mu\text{-}Me)_2AlMe_2\ B(C_6F_5)_4^-$ (7)

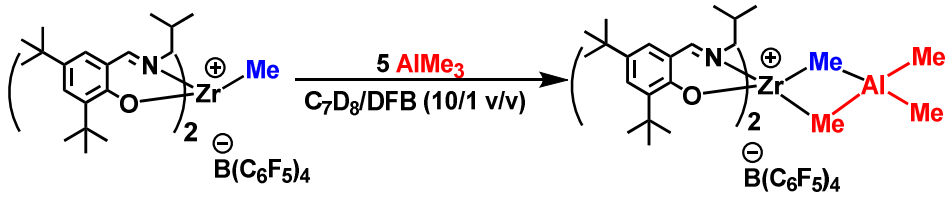

Proposed based on NMR

Procedure: In a glovebox, **FI_2ZrMe_2 (3)** (14.0 mg, 20 µmol, 1.0 equiv), BT (18.4 mg, 20 µmol, 1.0 equiv), C_7D_8 (0.472 g, 0.5 mL) and DFB (0.058 g, 0.05 mL) were added to a vial. The vial was capped and the mixture was shaken for 1 min, the solution was then transferred into an NMR tube equipped with Precision Seal® rubber septum cap, and removed from the glovebox immediately. To the solution in the NMR tube was added a solution of TMA in toluene (0.05 mL, 0.1 mmol, 5.0 equiv/Zr catalyst) immediately before performing NMR experiments. The cationic species was seen to decompose within 3 h, as indicated by color change from yellow to a dark red, as well as indecipherable peaks present in the NMR spectra. Thus, the NMR experiments were carried out at –50 ºC to minimize cationic species decomposition (additionally, low temperature NMR minimizes line broadening caused by fluxional coordination of the **FI** ligand to Zr).

The product and other species in the reaction mixture were identified, and thus the structure of **[Zr···Al](7)** is proposed based on ^{1}H NMR (**Figure S20**) and HSQC (**Figure S21**) spectra. An overlapping peak is observed with the bridging methyl group signal, Zr(µ-Me)$_2$AlMe$_2$. However, these peaks can be differentiated by HSQC (**Figure S21**). The coressponding chemical shifts are δ 0.95 ppm (^{1}H NMR) and 14.4 ppm (^{13}C NMR). The overlapping peak was identified as an impurity in the commercial TMA solution, as confirmed by control NMR experiments (**Figure S22**).

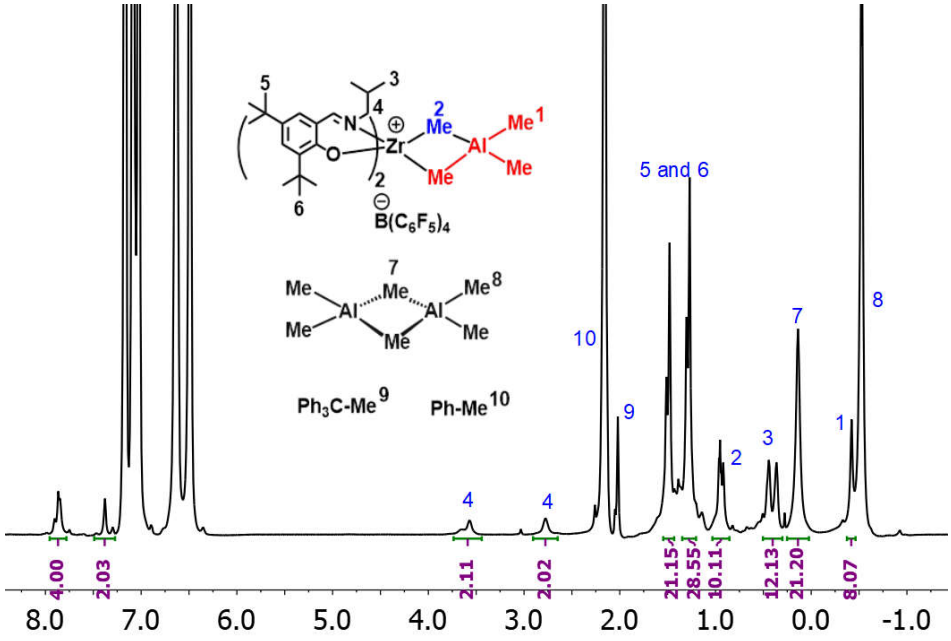

Figure S20. ^{1}H NMR spectra (600 MHz) of *in situ* generated **[Zr-Al](7)** (C_7D_8/DFB = 10/1, *v/v*, –50 °C). ^{1}H NMR peaks for Al_2Me_6, Ph_3C-Me and toluene are assigned.

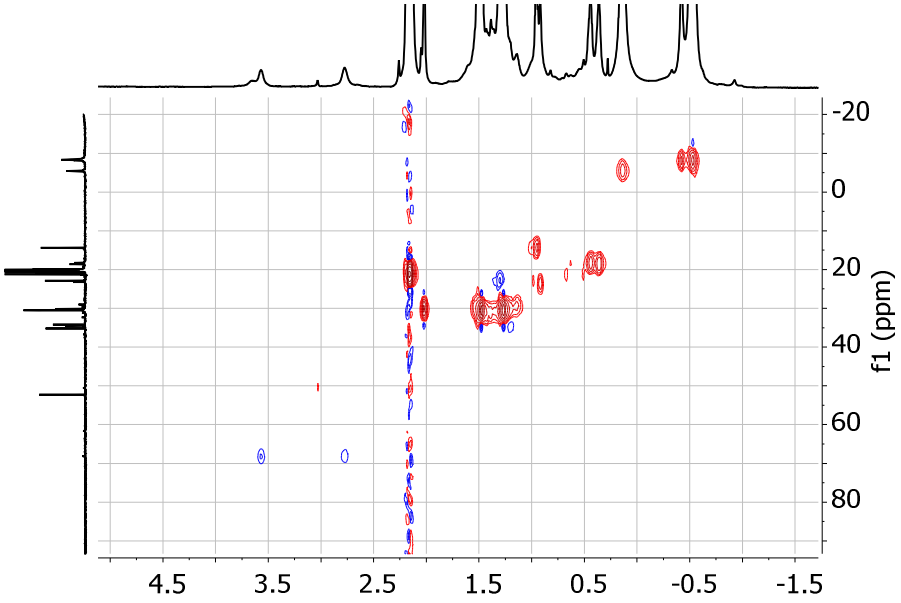

Figure S21. HSQC NMR spectra (600 MHz) of *in situ* generated **[Zr-Al](7)** (C_7D_8/DFB = 10/1, *v/v*, –50 °C); the solution also contains Al_2Me_6, Ph_3C-Me, and toluene.

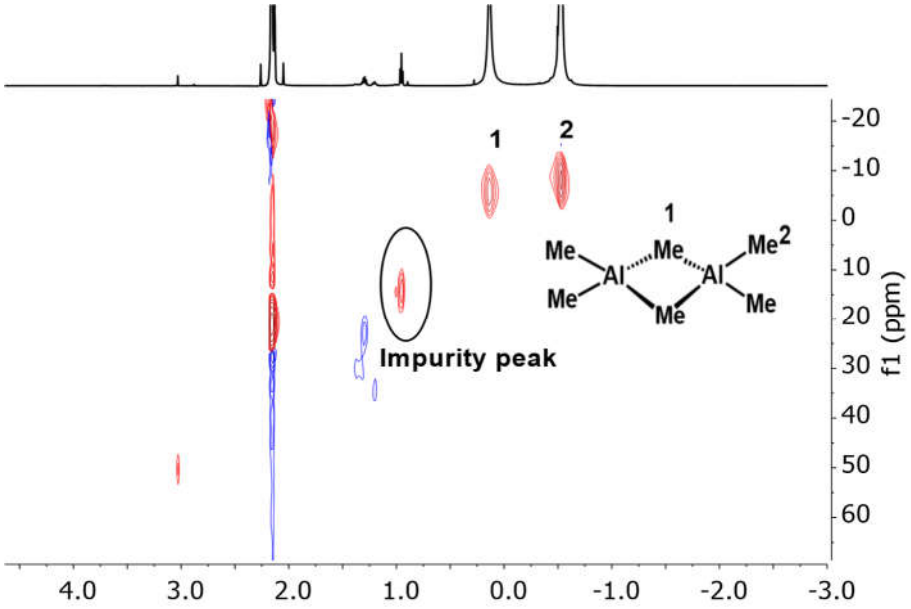

Figure S22. HSQC NMR spectra (600 MHz) of TMA (C_7D_8/DFB = 10/1, *v/v*, –50 ºC). In the solution: TMA (0.05 ml, 0.1 mmol, 2.0 M in toluene); C_7D_8 (0.472 g, 0.5 mL); DFB (0.058 g, 0.05 mL).

3) Reaction of FI_2ZrMe_2 (3) + TMA: Slow ancillary ligand transfer!

Procedure: In a glovebox, **FI_2ZrMe_2 (3)** (7.0 mg, 10 μmol, 1.0 equiv) and C_6D_6 (0.659 g, 0.7 mL) were added to a vial. The solution was then transferred into an NMR tube equipped with Precision Seal® rubber septum cap, and removed from the glovebox. TMA (0.025 mL, 0.05 mmol, 50 equiv) was added to the NMR tube via syringe. The NMR spectra were then recorded after 20 min. After 1 d, the same NMR experiments were recorded again for comparison. There is an obvious ^{1}H NMR chemical shift change upon addition of TMA, which indicates the coordination of TMA to **FI_2ZrMe_2 (3)**. **FI_2ZrMe_2 (3)** then undergoes slow ancillary ligand transfer in the presence of TMA, as indicated by the NMR comparison with **$FIAlMe_2$ (5)** + TMA (**Figure S23**). Peaks **A** and **B** represent $NCH_2CH\underline{(CH_3)_2}$ of the intact TMA-coordinated **FI_2ZrMe_2 (3)** and **$FIAlMe_2$ (5)**, respectively. Using Ph-*Me* (toluene from added TMA solution) as an internal reference, the NMR yield of ancillary ligand transfer product, **$FIAlMe_2$ (5),** is estimated to be approx 59%, while the remaining 41% is TMA-coordinated **FI_2ZrMe_2 (3)**.

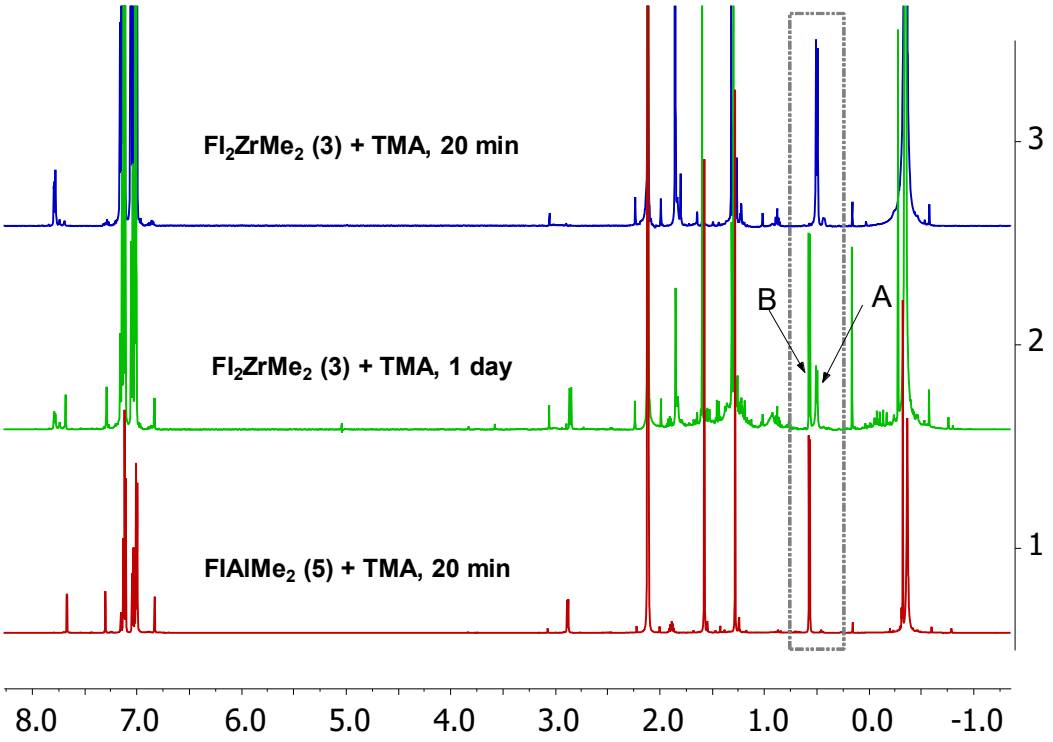

Figure S23. Comparison of ^{1}H NMR spectra (C_6D_6, 25 °C) (499 MHz): **FI_2ZrMe_2 (3)** + TMA mixing for 20 min vs. 1 d vs. **$FIAlMe_2$ (5)** + TMA mixing for 20 min. Peaks **A** and **B** represent $NCH_2CH\underline{(CH_3)_2}$ of the intact TMA-coordinated **FI_2ZrMe_2 (3)** and **$FIAlMe_2$ (5)**, respectively.

4) Reaction of $FI_2Zr(NMe_2)_2$ (1) + TMA vs. FI_2ZrMe_2 (3) + TMA and $FIAlMe_2$ (5) + TMA

The procedures for the three NMR reactions are the same, using **FI_2ZrMe_2 (3)** as an example: In a glovebox, **FI_2ZrMe_2 (3)** (14.0 mg, 20 μmol, 1.0 equiv), C_7D_8 (0.472 g, 0.5 mL), and DFB (0.058 g, 0.05 mL) were added to a vial. The vial was capped and then shaken for 1 min before the solution was transferred into an NMR tube equipped with Precision Seal® rubber septum cap, and removed from the glovebox. TMA (0.05 mL, 0.1 mmol, 100 equiv) was added to the NMR tube via syringe. NMR spectra were recorded after 30 min. The NMR comparison is shown in **Figure S24**.

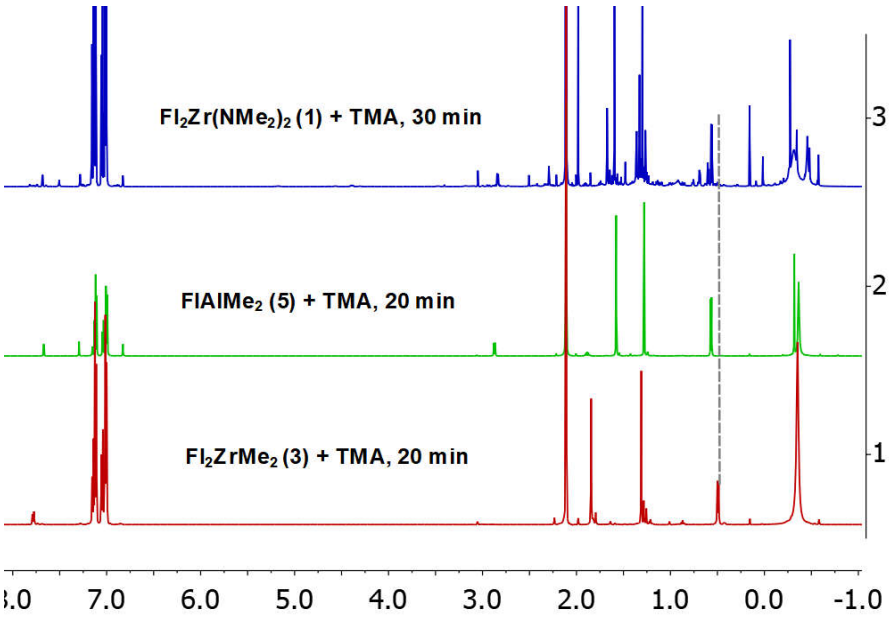

Figure S24. NMR spectra (499 MHz) of **$FI_2Zr(NMe_2)_2$ (1)** + TMA, **FI_2ZrMe_2 (3)** + TMA, Al (5) + TMA. (C_7D_8/DFB = 10/1, *v/v*, –50 °C).

Attempted Use of Mono-FI Precatalyst $FIZrBn_3$ as a Control

Mono-FI-Zr-alkyl complexes, i.e., $FIZrMe_3$ or $FIZrBn_3$, would be ideal models for a comparative study. Some mono-FI Zr complexes with bulky aromatic groups on the imine N are known in the literature such as: FI^*ZrBn_3,[11] FI^*TiMe_3,[12-13] $FI^*TiCl_3(THF)$,[14-16] and FI^*TiCl_3.[13] Note that these mono-FI* Ti or Zr complexes all have bulky aromatic substituents on the FI* ligand imine N. In contrast, the FI ligand in the present study has a less bulky isobutyl group on FI ligand imine N. While a $FI^*TiCl_3(THF)$ type Ti complex was reported with cyclohexyl group on imine N, the corresponding $FI^*ZrCl_3(THF)$ Zr complex is reported to be unstable even at low temperatures.[17] To the best of our knowledge, no mono-FIZr complex with less bulky aliphatic groups such as isobutyl on the FI imine N has yet been isolated.[16-19]

Several synthetic reactions were attempted with the aim of preparing the ideal model $FIZrR_3$ complex (R = Me, Bn) but were not successful. These include: 1. Reaction of HFI with 1 equiv of $ZrBn_4$; 2. Reaction of more bulky HFI* (methylcyclohexyl group on imine N) with 1 equiv of $ZrBn_4$; 3. Reaction of HFI with 5 equiv of in situ generated "$ZrMe_4$" from $ZrCl_4$ + 4MeMgBr, toluene at -78 °C;[20] 4. Further adding 10 equiv of TMA to the reaction mixture of reaction 3 at -78 °C in hope that TMA would assist in stabilizing $FIZrMe_3$ if it formed.

We also attempted to use the FI"BZrBn$_3$ complex reported by Chen *et al* (shown below)[11] as a control. It is known that substituents on the FI ligand imine N (alkyl vs. aromatic) exhibit dramatic effects on catalyst polymerization properties such as activity, comonomer selectivity, catalyst stability, etc.[19] However, in our hands this catalyst is barely active in ethylene/1-octene copolymerization under the following polymerization conditions: FI"ZrBn$_3$, 10 μmol, 7.6 mg; $Ph_3C^+B(C_6F_5)_4^-$, 11 μmol, 10.2 mg; 1-octene, 5 mL, 3.58 g; 1 atm ethylene; toluene, 45 mL; 40 ºC; reaction time, 3 min. Only 20 mg polymer is obtained for FI"ZrBn$_3$ vs. 2.37 g/0.5 min for FI$_2$ZrBn$_2$ (2) under the same conditions (Table 1, Entry 4 in the manuscript). The finding is not unexpected since dramatic FI imine N (alkyl vs. aromatic) substituent effects on the catalyst activity, comonomer selectivity, catalyst stability, etc., have been well established.[19] Thus, changing the R group on imine N from isobutyl to 2,6-diisopropylphenyl makes it possible to get the mono-FI Zr complex FI"ZrBn$_3$, however, it is a poor mono-FI control for this study.

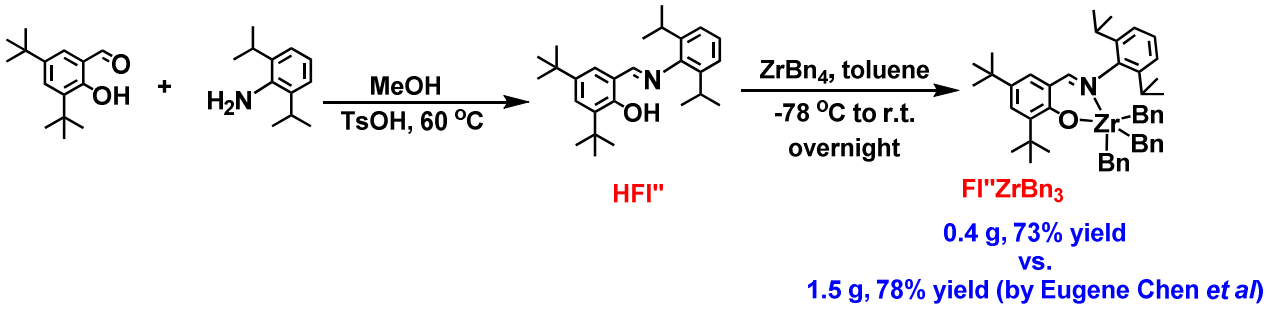

X-Ray Data Collection, Structure Solution, and Refinement

Single crystals of **FI$_2$Zr(NMe$_2$)$_2$ (1)**, **FI$_2$ZrMe$_2$ (3)**, **FI$_2$ZrCl$_2$ (4)**, **FIAlMe$_2$ (5)** and **FIZr(NMe$_2$)$_3$ (6)** were obtained from toluene/*n*-hexane, toluene, toluene, *n*-hexane, and pentane solution, respectively. A suitable crystal was selected and the crystal was mounted on a MITIGEN holder in Paratone oil on a Kappa Apex 2 diffractometer. The crystal was kept at 99.99 K during data collection. Using Olex2,[21] the structure was solved with the ShelXT[22] structure solution program using Intrinsic Phasing and refined with the ShelXL[23] refinement package using Least Squares minimization. The enhanced rigid-bond restraint (SHELX keyword RIGU) was applied globally.[24] Crystallographic and experimental details of the structure determination are summarized in **Table S1.** Bonds and angles are shown from **Table S2** to **Table S11**.

Table S1. Crystal data and structure refinement.

Complexes	1	3	4	5	6
Empirical formula	$C_{42}H_{72}N_4O_2Zr$	$C_{40}H_{66}N_2O_2Zr$	$C_{52}H_{76}Cl_2N_2O_2Zr$	$C_{23.5}H_{42}AlNO$	$C_{25}H_{48}N_4OZr$
FW	756.25	698.16	923.26	381.56	511.89
Temperature/K	99.99	100.02	99.99	100.0	100.0
Crystal system	monoclinic	tetragonal	monoclinic	monoclinic	triclinic
Space group	C2/c	$P4_3$	C2/c	C2/c	P-1
a / Å	22.969(2)	17.2175(7)	34.428(4)	20.2677(12)	9.5295(19)
b / Å	18.6514(16)	17.2175(7)	7.6685(8)	12.6644(8)	12.293(3)
c / Å	13.3922(12)	41.838(2)	20.142(2)	19.5770(12)	13.196(3)
α /°	90	90	90	90	103.64(3)
β / °	124.639(2)	90	102.221(3)	100.055(3)	98.59(3)
γ / °	90	90	90	90	105.65(3)
Volume / $Å^3$	4720.3(7)	12402.4(12)	5197.2(9)	4947.8(5)	1408.6(6)
Z	4	12	4	8	2
$\rho_{calcd}/(mg/mm^{-3})$	1.064	1.122	1.180	1.024	1.207
μ / mm^{-1}	2.154	0.298	2.960	0.782	0.412
F(000)	1632	4512	1968	1688	548.0
Crystal size / mm^3	0.364 × 0.146 × 0.054	0.093 × 0.073 × 0.017	0.226×0.091×0.066	0.379 × 0.286 × 0.256	0.249×0.172×0.092
2θ range for data collection	6.658 to 136.704°	1.946 to 51.39°	8.984 to 136.336°	8.268 to 133.344°	3.262 to 49.356°
Reflections collected	31709	126771	32616	14159	4683
Independent reflections	4192	23461	4716	4265	4683
Data/restraints/parameters	4192/0/232	23461/1162/1270	4716/380/418	4265/21/274	4683/0/326
Goodness-of-fit on F^2	1.052	1.086	1.071	1.126	1.055
Final R indices [I>2σ(I)]	R_1 = 0.0241, wR_2 = 0.0614	R_1 = 0.0706, wR_2 = 0.1616	R_1 = 0.0326, wR_2 = 0.0811	R_1 = 0.0443, wR_2 = 0.1121	R_1 = 0.0337, wR_2 = 0.0942
Final R indices [all data]	R_1 = 0.0244, wR_2 = 0.0616	R_1 = 0.0897, wR_2 = 0.1717	R_1 = 0.0342, wR_2 = 0.0827	R_1 = 0.0453, wR_2 = 0.1128	R_1 = 0.0365, wR_2 = 0.0967
Largest diff. Peak/hole/ e $Å^{-3}$	0.405/-0.467	0.894/-0.900	0.371/-0.900	0.357/-0.259	0.71/-0.60

Table S2. Bond Lengths (Å) for 1.

Atom	Atom	Length/Å	Atom	Atom	Length/Å
Zr1	$O1^1$	2.0357(10)	C3	C4	1.402(2)
Zr1	O1	2.0357(10)	C4	C5	1.380(2)

Zr1	N1	2.4371(12)	C4	C12	1.541(2)
Zr1	N1[1]	2.4370(12)	C5	C6	1.404(2)
Zr1	N2	2.0766(13)	C6	C7	1.452(2)
Zr1	N2[1]	2.0766(13)	C8	C9	1.538(2)
O1	C1	1.3240(18)	C8	C10	1.537(2)
N1	C7	1.287(2)	C8	C11	1.534(2)
N1	C16	1.4749(18)	C12	C13	1.523(3)
N2	C20	1.448(2)	C12	C14	1.522(3)
N2	C21	1.455(2)	C12	C15	1.515(3)
C1	C2	1.419(2)	C16	C17	1.535(2)
C1	C6	1.412(2)	C17	C18	1.529(2)
C2	C3	1.392(2)	C17	C19	1.522(2)
C2	C8	1.537(2)			

Table S3. Bond Angles (°) for 1.

Atom	Atom	Atom	Angle/°	Atom	Atom	Atom	Angle/°
O1[1]	Zr1	O1	156.69(6)	C3	C2	C8	122.00(14)
O1[1]	Zr1	N1[1]	76.08(4)	C2	C3	C4	124.58(15)
O1[1]	Zr1	N1	85.95(4)	C3	C4	C12	121.14(15)
O1	Zr1	N1[1]	85.95(4)	C5	C4	C3	116.58(14)
O1	Zr1	N1	76.08(4)	C5	C4	C12	122.15(15)
O1[1]	Zr1	N2	94.12(5)	C4	C5	C6	121.88(14)
O1[1]	Zr1	N2[1]	101.39(5)	C1	C6	C7	122.82(13)
O1	Zr1	N2	101.39(5)	C5	C6	C1	120.21(14)
O1	Zr1	N2[1]	94.12(5)	C5	C6	C7	116.72(13)
N1[1]	Zr1	N1	79.26(6)	N1	C7	C6	128.65(13)
N2	Zr1	N1[1]	92.24(5)	C2	C8	C9	109.22(12)
N2[1]	Zr1	N1[1]	171.23(5)	C2	C8	C10	111.04(13)
N2	Zr1	N1	171.23(5)	C10	C8	C9	110.15(14)

N2[1]	Zr1	N1	92.24(5)	C11	C8	C2	111.87(14)
N2	Zr1	N2[1]	96.34(7)	C11	C8	C9	107.23(14)
C1	O1	Zr1	145.28(9)	C11	C8	C10	107.25(13)
C7	N1	Zr1	124.78(10)	C13	C12	C4	111.79(15)
C7	N1	C16	114.70(12)	C14	C12	C4	108.71(14)
C16	N1	Zr1	120.45(9)	C14	C12	C13	107.43(18)
C20	N2	Zr1	127.60(11)	C15	C12	C4	111.34(15)
C20	N2	C21	111.03(13)	C15	C12	C13	110.4(2)
C21	N2	Zr1	121.05(11)	C15	C12	C14	107.0(2)
O1	C1	C2	121.17(13)	N1	C16	C17	112.44(12)
O1	C1	C6	119.68(13)	C18	C17	C16	108.78(13)
C6	C1	C2	119.14(13)	C19	C17	C16	111.90(13)
C1	C2	C8	120.47(13)	C19	C17	C18	109.97(13)
C3	C2	C1	117.46(14)				

Table S4. Bond Lengths (Å) for 3.

Atom	Atom	Length/Å	Atom	Atom	Length/Å
Zr1	O1	2.013(9)	C13A	C14A	1.516(19)
Zr1	O2	1.998(9)	C13A	C15A	1.536(16)
Zr1	N1	2.403(11)	C13A	C16A	1.555(18)
Zr1	N2	2.402(10)	C18A	C19A	1.501(17)
Zr1	C1	2.282(13)	C19A	C20A	1.49(2)
Zr1	C2	2.261(13)	C19A	C21A	1.561(17)
O1	C3	1.321(15)	C22A	C23A	1.432(16)
O2	C22	1.367(16)	C22A	C27A	1.368(17)
N1	C17	1.330(16)	C23A	C24A	1.371(17)
N1	C18	1.497(15)	C23A	C28A	1.522(17)
N2	C36	1.284(16)	C24A	C25A	1.408(18)
N2	C37	1.466(16)	C25A	C26A	1.372(18)

C3	C4	1.409(16)	C25A	C32A	1.515(17)
C3	C8	1.425(17)	C26A	C27A	1.441(17)
C4	C5	1.373(18)	C27A	C36A	1.425(16)
C4	C9	1.553(18)	C28A	C29A	1.517(19)
C5	C6	1.451(19)	C28A	C30A	1.50(2)
C6	C7	1.366(18)	C28A	C31A	1.559(18)
C6	C13	1.526(19)	C32A	C33A	1.53(2)
C7	C8	1.424(18)	C32A	C34A	1.519(18)
C8	C17	1.407(17)	C32A	C35A	1.53(2)
C9	C10	1.540(19)	C37A	C38A	1.513(18)
C9	C11	1.530(19)	C38A	C39A	1.49(2)
C9	C12	1.502(19)	C38A	C40A	1.499(19)
C13	C14	1.54(2)	Zr1B	O1B	1.991(9)
C13	C15	1.522(18)	Zr1B	O2B	2.014(8)
C13	C16	1.54(2)	Zr1B	N1B	2.419(11)
C18	C19	1.521(18)	Zr1B	N2B	2.398(10)
C19	C20	1.51(2)	Zr1B	C1B	2.299(13)
C19	C21	1.526(19)	Zr1B	C2B	2.269(13)
C22	C23	1.387(18)	O1B	C3B	1.362(15)
C22	C27	1.408(17)	O2B	C22B	1.315(15)
C23	C24	1.418(17)	N1B	C17B	1.284(16)
C23	C28	1.555(18)	N1B	C18B	1.427(16)
C24	C25	1.403(17)	N2B	C36B	1.322(15)
C25	C26	1.400(18)	N2B	C37B	1.478(16)
C25	C32	1.512(18)	C3B	C4B	1.419(17)
C26	C27	1.370(17)	C3B	C8B	1.392(17)
C27	C36	1.427(17)	C4B	C5B	1.381(18)
C28	C29	1.52(2)	C4B	C9B	1.531(18)

C28	C30	1.54(2)	C5B	C6B	1.377(18)
C28	C31	1.482(19)	C6B	C7B	1.418(19)
C32	C33	1.53(2)	C6B	C13B	1.548(18)
C32	C34	1.572(19)	C7B	C8B	1.360(18)
C32	C35	1.54(2)	C8B	C17B	1.485(18)
C37	C38	1.534(19)	C9B	C10B	1.52(2)
C38	C39	1.54(2)	C9B	C11B	1.54(2)
C38	C40	1.52(2)	C9B	C12B	1.51(2)
Zr1A	O1A	1.996(8)	C13B	C14B	1.50(2)
Zr1A	O2A	2.017(8)	C13B	C15B	1.54(2)
Zr1A	N1A	2.407(10)	C13B	C16B	1.48(2)
Zr1A	N2A	2.424(10)	C18B	C19B	1.535(17)
Zr1A	C1A	2.304(12)	C19B	C20B	1.530(19)
Zr1A	C2A	2.275(12)	C19B	C21B	1.534(18)
O1A	C3A	1.351(15)	C22B	C23B	1.439(17)
O2A	C22A	1.312(15)	C22B	C27B	1.399(17)
N1A	C17A	1.253(15)	C23B	C24B	1.356(17)
N1A	C18A	1.480(15)	C23B	C28B	1.548(17)
N2A	C36A	1.294(15)	C24B	C25B	1.420(18)
N2A	C37A	1.453(15)	C25B	C26B	1.412(17)
C3A	C4A	1.427(16)	C25B	C32B	1.536(18)
C3A	C8A	1.404(16)	C26B	C27B	1.410(17)
C4A	C5A	1.382(17)	C27B	C36B	1.444(17)
C4A	C9A	1.540(16)	C28B	C29B	1.535(19)
C5A	C6A	1.376(17)	C28B	C30B	1.532(19)
C6A	C7A	1.409(17)	C28B	C31B	1.575(18)
C6A	C13A	1.521(18)	C32B	C33B	1.550(19)
C7A	C8A	1.372(17)	C32B	C34B	1.517(19)

C8A	C17A	1.473(17)	C32B	C35B	1.501(19)
C9A	C10A	1.555(17)	C37B	C38B	1.523(17)
C9A	C11A	1.563(17)	C38B	C39B	1.516(17)
C9A	C12A	1.544(17)	C38B	C40B	1.559(18)

Table S5. Bond Angles (°) for 3.

Atom	Atom	Atom	Angle/°	Atom	Atom	Atom	Angle/°
O1	Zr1	N1	76.2(3)	C6A	C13A	C15A	109.9(10)
O1	Zr1	N2	97.0(4)	C6A	C13A	C16A	111.3(11)
O1	Zr1	C1	95.0(4)	C14A	C13A	C6A	109.0(11)
O1	Zr1	C2	89.0(5)	C14A	C13A	C15A	111.3(12)
O2	Zr1	O1	172.6(4)	C14A	C13A	C16A	106.5(11)
O2	Zr1	N1	100.2(4)	C15A	C13A	C16A	108.8(11)
O2	Zr1	N2	75.7(4)	N1A	C17A	C8A	128.1(11)
O2	Zr1	C1	91.4(4)	N1A	C18A	C19A	112.5(10)
O2	Zr1	C2	93.5(5)	C18A	C19A	C21A	109.8(11)
N2	Zr1	N1	72.9(4)	C20A	C19A	C18A	112.5(11)
C1	Zr1	N1	89.4(5)	C20A	C19A	C21A	112.0(11)
C1	Zr1	N2	155.5(4)	O2A	C22A	C23A	119.9(11)
C2	Zr1	N1	162.9(5)	O2A	C22A	C27A	120.1(11)
C2	Zr1	N2	101.0(5)	C27A	C22A	C23A	119.9(12)
C2	Zr1	C1	100.5(6)	C22A	C23A	C28A	120.3(11)
C3	O1	Zr1	145.7(8)	C24A	C23A	C22A	116.3(11)
C22	O2	Zr1	146.5(8)	C24A	C23A	C28A	123.3(11)
C17	N1	Zr1	126.7(8)	C23A	C24A	C25A	126.1(12)
C17	N1	C18	116.1(11)	C24A	C25A	C32A	119.1(12)
C18	N1	Zr1	117.1(8)	C26A	C25A	C24A	116.3(12)
C36	N2	Zr1	125.9(9)	C26A	C25A	C32A	124.6(12)
C36	N2	C37	116.1(11)	C25A	C26A	C27A	120.3(12)

C37	N2	Zr1	118.0(8)	C22A	C27A	C26A	120.9(11)
O1	C3	C4	121.0(11)	C22A	C27A	C36A	123.3(11)
O1	C3	C8	119.1(11)	C36A	C27A	C26A	115.7(11)
C4	C3	C8	119.9(12)	C23A	C28A	C31A	110.5(10)
C3	C4	C9	120.6(12)	C29A	C28A	C23A	112.5(11)
C5	C4	C3	118.9(12)	C29A	C28A	C31A	108.2(11)
C5	C4	C9	120.5(11)	C30A	C28A	C23A	109.9(11)
C4	C5	C6	122.8(12)	C30A	C28A	C29A	110.2(11)
C5	C6	C13	117.9(11)	C30A	C28A	C31A	105.3(12)
C7	C6	C5	117.6(12)	C25A	C32A	C33A	111.1(12)
C7	C6	C13	124.3(12)	C25A	C32A	C34A	109.3(11)
C6	C7	C8	121.5(12)	C25A	C32A	C35A	111.4(11)
C7	C8	C3	119.4(11)	C33A	C32A	C35A	108.4(12)
C17	C8	C3	124.3(11)	C34A	C32A	C33A	108.9(12)
C17	C8	C7	116.2(11)	C34A	C32A	C35A	107.6(12)
C10	C9	C4	112.0(11)	N2A	C36A	C27A	127.9(12)
C11	C9	C4	107.5(10)	N2A	C37A	C38A	113.0(11)
C11	C9	C10	108.7(12)	C39A	C38A	C37A	114.5(12)
C12	C9	C4	111.3(11)	C39A	C38A	C40A	109.8(12)
C12	C9	C10	105.9(11)	C40A	C38A	C37A	110.7(12)
C12	C9	C11	111.5(12)	O1B	Zr1B	O2B	170.9(3)
C6	C13	C14	110.5(12)	O1B	Zr1B	N1B	76.5(3)
C6	C13	C16	111.4(11)	O1B	Zr1B	N2B	95.1(3)
C14	C13	C16	110.2(13)	O1B	Zr1B	C1B	96.6(4)
C15	C13	C6	108.3(12)	O1B	Zr1B	C2B	90.0(4)
C15	C13	C14	109.1(13)	O2B	Zr1B	N1B	98.0(4)
C15	C13	C16	107.2(12)	O2B	Zr1B	N2B	76.2(3)
N1	C17	C8	126.6(11)	O2B	Zr1B	C1B	90.5(4)
N1	C18	C19	113.4(11)	O2B	Zr1B	C2B	94.0(4)

C18	C19	C21	107.1(12)	N2B	Zr1B	N1B	72.9(3)
C20	C19	C18	111.6(12)	C1B	Zr1B	N1B	88.8(5)
C20	C19	C21	111.1(13)	C1B	Zr1B	N2B	155.2(5)
O2	C22	C23	119.2(11)	C2B	Zr1B	N1B	163.0(5)
O2	C22	C27	118.2(11)	C2B	Zr1B	N2B	98.6(5)
C23	C22	C27	122.6(12)	C2B	Zr1B	C1B	103.1(6)
C22	C23	C24	116.1(12)	C3B	O1B	Zr1B	145.8(8)
C22	C23	C28	124.6(11)	C22B	O2B	Zr1B	145.9(8)
C24	C23	C28	119.3(11)	C17B	N1B	Zr1B	125.4(8)
C25	C24	C23	123.0(12)	C17B	N1B	C18B	115.5(11)
C24	C25	C32	118.7(12)	C18B	N1B	Zr1B	118.9(8)
C26	C25	C24	117.4(12)	C36B	N2B	Zr1B	126.7(8)
C26	C25	C32	123.9(12)	C36B	N2B	C37B	114.5(10)
C27	C26	C25	121.9(12)	C37B	N2B	Zr1B	118.7(8)
C22	C27	C36	121.9(12)	O1B	C3B	C4B	119.9(11)
C26	C27	C22	119.0(12)	O1B	C3B	C8B	119.5(11)
C26	C27	C36	118.9(12)	C8B	C3B	C4B	120.6(12)
C29	C28	C23	110.0(12)	C3B	C4B	C9B	121.5(12)
C29	C28	C30	106.4(11)	C5B	C4B	C3B	115.3(12)
C30	C28	C23	108.3(11)	C5B	C4B	C9B	123.1(12)
C31	C28	C23	113.5(11)	C6B	C5B	C4B	125.7(13)
C31	C28	C29	109.9(12)	C5B	C6B	C7B	116.7(12)
C31	C28	C30	108.3(13)	C5B	C6B	C13B	119.6(12)
C25	C32	C33	109.0(11)	C7B	C6B	C13B	123.5(12)
C25	C32	C34	108.7(11)	C8B	C7B	C6B	120.0(13)
C25	C32	C35	113.1(12)	C3B	C8B	C17B	121.4(11)
C33	C32	C34	109.1(12)	C7B	C8B	C3B	121.4(12)
C33	C32	C35	107.2(12)	C7B	C8B	C17B	117.0(11)
C35	C32	C34	109.7(12)	C4B	C9B	C11B	112.1(12)

N2	C36	C27	130.4(12)	C10B	C9B	C4B	111.0(12)
N2	C37	C38	114.5(12)	C10B	C9B	C11B	106.4(13)
C37	C38	C39	108.0(12)	C12B	C9B	C4B	109.9(12)
C40	C38	C37	113.3(13)	C12B	C9B	C10B	107.2(13)
C40	C38	C39	110.5(13)	C12B	C9B	C11B	110.0(12)
O1A	Zr1A	O2A	171.0(3)	C14B	C13B	C6B	108.1(12)
O1A	Zr1A	N1A	75.8(3)	C14B	C13B	C15B	108.1(14)
O1A	Zr1A	N2A	96.6(3)	C15B	C13B	C6B	106.5(12)
O1A	Zr1A	C1A	96.9(4)	C16B	C13B	C6B	112.1(13)
O1A	Zr1A	C2A	89.2(4)	C16B	C13B	C14B	109.8(14)
O2A	Zr1A	N1A	98.4(3)	C16B	C13B	C15B	112.1(14)
O2A	Zr1A	N2A	75.0(3)	N1B	C17B	C8B	129.3(12)
O2A	Zr1A	C1A	90.2(4)	N1B	C18B	C19B	114.6(11)
O2A	Zr1A	C2A	94.8(4)	C20B	C19B	C18B	110.5(11)
N1A	Zr1A	N2A	73.3(3)	C20B	C19B	C21B	110.7(12)
C1A	Zr1A	N1A	93.5(5)	C21B	C19B	C18B	110.4(11)
C1A	Zr1A	N2A	158.1(4)	O2B	C22B	C23B	121.1(11)
C2A	Zr1A	N1A	160.4(5)	O2B	C22B	C27B	119.5(11)
C2A	Zr1A	N2A	96.4(5)	C27B	C22B	C23B	119.3(11)
C2A	Zr1A	C1A	100.9(6)	C22B	C23B	C28B	118.2(11)
C3A	O1A	Zr1A	146.2(7)	C24B	C23B	C22B	117.4(11)
C22A	O2A	Zr1A	146.1(7)	C24B	C23B	C28B	123.7(11)
C17A	N1A	Zr1A	127.6(8)	C23B	C24B	C25B	125.3(12)
C17A	N1A	C18A	117.6(10)	C24B	C25B	C32B	120.3(11)
C18A	N1A	Zr1A	114.6(8)	C26B	C25B	C24B	116.4(11)
C36A	N2A	Zr1A	125.9(8)	C26B	C25B	C32B	123.3(11)
C36A	N2A	C37A	118.7(10)	C27B	C26B	C25B	120.0(12)
C37A	N2A	Zr1A	115.4(7)	C22B	C27B	C26B	121.3(11)
O1A	C3A	C4A	120.3(10)	C22B	C27B	C36B	123.9(11)

O1A	C3A	C8A	119.3(10)	C26B	C27B	C36B	114.8(11)
C8A	C3A	C4A	120.3(11)	C23B	C28B	C31B	109.2(10)
C3A	C4A	C9A	121.3(11)	C29B	C28B	C23B	110.6(11)
C5A	C4A	C3A	115.5(11)	C29B	C28B	C31B	106.2(11)
C5A	C4A	C9A	123.2(10)	C30B	C28B	C23B	109.4(11)
C6A	C5A	C4A	126.9(12)	C30B	C28B	C29B	111.6(12)
C5A	C6A	C7A	114.8(12)	C30B	C28B	C31B	109.8(12)
C5A	C6A	C13A	120.2(11)	C25B	C32B	C33B	107.1(11)
C7A	C6A	C13A	124.8(12)	C34B	C32B	C25B	107.2(11)
C8A	C7A	C6A	122.8(12)	C34B	C32B	C33B	111.9(12)
C3A	C8A	C17A	121.8(11)	C35B	C32B	C25B	113.4(11)
C7A	C8A	C3A	119.6(11)	C35B	C32B	C33B	110.4(12)
C7A	C8A	C17A	118.6(11)	C35B	C32B	C34B	106.9(12)
C4A	C9A	C10A	112.1(10)	N2B	C36B	C27B	126.2(11)
C4A	C9A	C11A	108.5(9)	N2B	C37B	C38B	111.4(10)
C4A	C9A	C12A	111.0(10)	C37B	C38B	C40B	107.0(11)
C10A	C9A	C11A	108.0(11)	C39B	C38B	C37B	113.4(11)
C12A	C9A	C10A	107.5(10)	C39B	C38B	C40B	111.0(11)
C12A	C9A	C11A	109.7(10)				

Table S6. Bond Lengths (Å) for 4.

Atom	Atom	Length/Å	Atom	Atom	Length/Å
Zr1	Cl1	2.4312(6)	C7	C10	1.538(3)
Zr1	Cl1[1]	2.4312(6)	C11	C12	1.537(5)
Zr1	O1	1.9926(13)	C11	C13	1.536(5)
Zr1	O1[1]	1.9927(13)	C11	C14	1.537(6)
Zr1	N1[1]	2.3260(18)	C11A	C12A	1.532(6)
Zr1	N1	2.3260(18)	C11A	C13A	1.539(6)

O1	C1	1.340(3)	C11A	C14A	1.520(6)
N1	C15	1.292(3)	C16	C17	1.520(4)
N1	C16	1.478(3)	C17	C18	1.534(3)
C1	C2	1.416(3)	C17	C19	1.527(4)
C1	C6	1.399(4)	C20	C21	1.371(7)
C2	C3	1.343(5)	C20	C25	1.378(10)
C2	C3A	1.478(5)	C20	C26	1.377(10)
C2	C7	1.527(4)	C21	C22	1.372(9)
C3	C4	1.389(6)	C22	C23	1.344(8)
C3A	C4A	1.413(5)	C23	C24	1.404(8)
C4	C5	1.386(5)	C24	C25	1.390(11)
C4	C11	1.537(7)	C25	C26B	1.584(17)
C4A	C5A	1.398(5)	C20A	C21A	1.390(8)
C4A	C11A	1.542(7)	C20A	C25A	1.404(9)
C5	C6	1.401(5)	C20A	C26A	1.493(9)
C5A	C6	1.459(5)	C21A	C22A	1.379(8)
C6	C15	1.446(3)	C22A	C23A	1.383(8)
C7	C8	1.534(4)	C23A	C24A	1.389(9)
C7	C9	1.535(3)	C24A	C25A	1.406(11)

Table S7. Bond Angles (°) for 4.

Atom	Atom	Atom	Angle/°	Atom	Atom	Atom	Angle/°
Cl1	Zr1	Cl1[1]	102.79(3)	C2	C7	C8	109.46(19)
O1	Zr1	Cl1	92.68(5)	C2	C7	C9	112.2(2)
O1	Zr1	Cl1[1]	95.26(4)	C2	C7	C10	111.4(2)
O1[1]	Zr1	Cl1[1]	92.68(5)	C8	C7	C9	109.0(3)

O1[1]	Zr1	Cl1	95.26(4)	C8	C7	C10	107.8(2)
O1	Zr1	O1[1]	167.26(8)	C9	C7	C10	106.8(2)
O1[1]	Zr1	N1[1]	77.83(6)	C4	C11	C14	112.8(4)
O1	Zr1	N1	77.83(6)	C12	C11	C4	108.9(4)
O1	Zr1	N1[1]	92.04(6)	C12	C11	C14	108.6(4)
O1[1]	Zr1	N1	92.04(6)	C13	C11	C4	108.5(4)
N1	Zr1	Cl1[1]	91.45(5)	C13	C11	C12	109.2(4)
N1[1]	Zr1	Cl1	91.45(5)	C13	C11	C14	108.9(5)
N1	Zr1	Cl1	163.63(5)	C12A	C11A	C4A	109.0(4)
N1[1]	Zr1	Cl1[1]	163.63(5)	C12A	C11A	C13A	108.6(4)
N1[1]	Zr1	N1	75.79(10)	C13A	C11A	C4A	109.0(5)
C1	O1	Zr1	144.26(15)	C14A	C11A	C4A	110.9(4)
C15	N1	Zr1	126.42(16)	C14A	C11A	C12A	112.1(6)
C15	N1	C16	115.97(19)	C14A	C11A	C13A	107.1(5)
C16	N1	Zr1	117.58(13)	N1	C15	C6	128.4(2)
O1	C1	C2	120.7(2)	N1	C16	C17	111.9(2)
O1	C1	C6	118.80(18)	C16	C17	C18	109.1(3)
C6	C1	C2	120.5(2)	C16	C17	C19	112.8(2)
C1	C2	C3A	109.2(3)	C19	C17	C18	111.1(2)
C1	C2	C7	122.0(2)	C21	C20	C25	119.2(6)
C3	C2	C1	124.5(3)	C21	C20	C26	126.1(8)
C3	C2	C7	113.3(3)	C26	C20	C25	114.7(7)
C3A	C2	C7	128.2(3)	C20	C21	C22	121.4(6)
C2	C3	C4	115.9(5)	C23	C22	C21	119.8(5)
C4A	C3A	C2	132.4(4)	C22	C23	C24	120.9(6)
C3	C4	C11	117.8(4)	C25	C24	C23	118.5(6)
C5	C4	C3	120.0(5)	C20	C25	C24	120.3(6)
C5	C4	C11	122.2(5)	C20	C25	C26B	102.6(9)

C3A	C4A	C11A	121.5(4)	C24	C25	C26B	137.1(10)
C5A	C4A	C3A	114.9(4)	C21A	C20A	C25A	119.1(6)
C5A	C4A	C11A	123.7(4)	C21A	C20A	C26A	121.2(5)
C4	C5	C6	125.3(5)	C25A	C20A	C26A	119.7(6)
C4A	C5A	C6	115.3(4)	C22A	C21A	C20A	121.6(5)
C1	C6	C5	112.5(3)	C21A	C22A	C23A	120.3(6)
C1	C6	C5A	127.0(3)	C22A	C23A	C24A	118.9(5)
C1	C6	C15	122.51(19)	C23A	C24A	C25A	121.6(5)
C5	C6	C15	124.4(3)	C20A	C25A	C24A	118.5(7)
C15	C6	C5A	109.3(3)				

Table S8. Bond Lengths (Å) for 5.

Atom	Atom	Length/Å	Atom	Atom	Length/Å
Al1	O1	1.7746(12)	C8	C9	1.447(2)
Al1	N1	1.9677(14)	C10	C11	1.541(2)
Al1	C1	1.9579(19)	C10	C12	1.537(2)
Al1	C2	1.9558(19)	C10	C13	1.530(2)
O1	C3	1.3303(19)	C14	C15	1.535(2)
N1	C9	1.295(2)	C14	C16	1.532(2)
N1	C18	1.472(2)	C14	C17	1.529(2)
C3	C4	1.420(2)	C18	C19	1.531(2)
C3	C8	1.415(2)	C19	C20	1.523(2)
C4	C5	1.388(2)	C19	C21	1.518(2)
C4	C10	1.542(2)	C22	C23	1.458(12)
C5	C6	1.409(2)	C23	C24	1.481(10)
C6	C7	1.373(2)	C24	C25	1.559(8)
C6	C14	1.538(2)	C25	C26	1.487(6)

C7	C8	1.412(2)

Table S9. Bond Angles (°) for 5.

Atom	Atom	Atom	Angle/°	Atom	Atom	Atom	Angle/°
O1	Al1	N1	94.11(5)	C7	C8	C3	120.64(14)
O1	Al1	C1	110.74(7)	C7	C8	C9	116.66(14)
O1	Al1	C2	111.44(8)	N1	C9	C8	126.64(14)
C1	Al1	N1	108.26(7)	C11	C10	C4	109.49(13)
C2	Al1	N1	109.63(7)	C12	C10	C4	110.49(13)
C2	Al1	C1	119.61(9)	C12	C10	C11	109.80(14)
C3	O1	Al1	126.62(10)	C13	C10	C4	111.95(13)
C9	N1	Al1	119.35(11)	C13	C10	C11	107.58(14)
C9	N1	C18	118.33(13)	C13	C10	C12	107.47(14)
C18	N1	Al1	122.27(10)	C15	C14	C6	109.15(13)
O1	C3	C4	120.78(14)	C16	C14	C6	109.77(14)
O1	C3	C8	120.27(14)	C16	C14	C15	109.49(15)
C8	C3	C4	118.90(14)	C17	C14	C6	111.86(13)
C3	C4	C10	120.76(13)	C17	C14	C15	108.16(14)
C5	C4	C3	117.48(14)	C17	C14	C16	108.38(15)
C5	C4	C10	121.74(14)	N1	C18	C19	112.72(12)
C4	C5	C6	124.75(14)	C20	C19	C18	108.54(13)
C5	C6	C14	119.95(14)	C21	C19	C18	111.66(13)
C7	C6	C5	116.84(14)	C21	C19	C20	111.60(14)
C7	C6	C14	123.21(14)	C22	C23	C24	116.4(10)
C6	C7	C8	121.39(14)	C23	C24	C25	111.9(8)
C3	C8	C9	122.55(14)	C26	C25	C24	110.4(5)

Table S10. Bond Lengths (Å) for 6.

Atom	Atom	Length/Å	Atom	Atom	Length/Å
Zr1	O1	2.0466(18)	C3	C4	1.396(4)
Zr1	N1	2.393(2)	C4	C5	1.388(4)
Zr1	N2	2.042(2)	C4	C11	1.535(4)
Zr1	N3	2.046(3)	C5	C6	1.401(4)
Zr1	N4	2.079(3)	C6	C15	1.445(4)
O1	C1	1.329(3)	C7	C8	1.538(4)
N1	C15	1.289(3)	C7	C9	1.535(4)
N1	C16	1.471(3)	C7	C10	1.533(4)
N2	C20	1.453(4)	C11	C3A	1.624(7)
N2	C21	1.463(4)	C11	C5A	1.562(6)
N3	C22	1.452(4)	C11	C6A	1.469(6)
N3	C23	1.453(4)	C11	C12	1.541(6)
N4	C24	1.454(4)	C11	C14	1.403(7)
N4	C25	1.461(4)	C11	C13	1.613(7)
C1	C2	1.419(4)	C16	C17	1.532(4)
C1	C6	1.415(4)	C17	C18	1.516(4)
C2	C3	1.395(4)	C17	C19	1.518(5)
C2	C7	1.537(4)			

Table S11. Bond Angles (°) for 6.

Atom	Atom	Atom	Angle/°	Atom	Atom	Atom	Angle/°
O1	Zr1	N1	75.11(8)	C3	C4	C11	121.3(2)
O1	Zr1	N4	95.06(9)	C5	C4	C3	117.1(2)
N2	Zr1	O1	134.58(9)	C5	C4	C11	121.6(3)
N2	Zr1	N1	81.98(8)	C4	C5	C6	121.2(3)
N2	Zr1	N3	112.30(10)	C1	C6	C15	121.8(2)

N2	Zr1	N4	93.24(10)	C5	C6	C1	120.7(2)
N3	Zr1	O1	109.04(9)	C5	C6	C15	117.3(2)
N3	Zr1	N1	96.96(10)	C2	C7	C8	110.8(2)
N3	Zr1	N4	103.11(11)	C9	C7	C2	111.9(2)
N4	Zr1	N1	159.68(9)	C9	C7	C8	106.6(2)
C1	O1	Zr1	141.29(16)	C10	C7	C2	109.4(2)
C15	N1	Zr1	125.49(18)	C10	C7	C8	110.2(3)
C15	N1	C16	116.0(2)	C10	C7	C9	108.0(2)
C16	N1	Zr1	118.31(16)	C4	C11	C3A	109.5(3)
C20	N2	Zr1	130.74(19)	C4	C11	C5A	111.0(3)
C20	N2	C21	110.9(2)	C4	C11	C12	106.9(3)
C21	N2	Zr1	118.14(19)	C4	C11	C13	105.2(3)
C22	N3	Zr1	127.5(2)	C5A	C11	C3A	103.0(4)
C22	N3	C23	111.2(2)	C6A	C11	C4	116.2(3)
C23	N3	Zr1	121.2(2)	C6A	C11	C3A	105.8(4)
C24	N4	Zr1	118.2(2)	C6A	C11	C5A	110.3(4)
C24	N4	C25	110.2(3)	C12	C11	C13	106.1(4)
C25	N4	Zr1	131.4(2)	C14	C11	C4	114.1(3)
O1	C1	C2	121.3(2)	C14	C11	C12	114.3(4)
O1	C1	C6	119.9(2)	C14	C11	C13	109.7(4)
C6	C1	C2	118.8(2)	N1	C15	C6	127.5(3)
C1	C2	C7	120.8(2)	N1	C16	C17	112.0(2)
C3	C2	C1	117.6(2)	C18	C17	C16	109.6(3)
C3	C2	C7	121.5(2)	C18	C17	C19	111.3(3)
C2	C3	C4	124.3(2)	C19	C17	C16	111.7(3)

Buried Volume Calculations

Buried volume calculation (https://www.molnac.unisa.it/OMtools/sambvca2.0/index.html) gives a measure of the space occupied by the ligand in the first coordination sphere of the metal in transition metal complexes.[25] Thus, crystal structures of **1** and **6** were used as models to calculate

the percentage buried volume, $\%V_{Bur}$, for the ligand backbones of bis-**FI** and mono-**FI** catalysts. The radius (R) of the sphere around the metal center was set to 3.5 Å and a mesh of 0.1 Å was used to scan the sphere. NMe_2 groups remaining on the Zr of **1** and **6** were removed in order to analyze the influence of the ancillary ligand only. As discussed above, we proposed that the unusual catalyst precursor effects on comonomer incorporation are due to the reduced steric bulk around Zr after abstraction of one **FI** ligand by TMA from **1** during the alkylation step. Thus, we evaluated steric crowding maps of mono- and bis-**FI** ligated Zr catalysts by performing buried volume calculations.[28] The percentage buried volume, %VBur, for the backbones of bis-**FI** and mono-**FI** catalysts within a radius of 3.5 Å around the metal center was calculated. The %VBur for the **FI**$_2$Zr backbone is significantly higher (77.4%) than the **FI**Zr backbone (58.9%), suggesting the mono-**FI** ligated Zr catalyst is far less bulky than the bis-**FI** ligated Zr catalyst. This makes coordination of the 1-octene comonomer more selective. This likely explains the high incorporation capacity of mono-ligated **FI**Zr catalysts that are generated from the TMA-alkylations of **1** and **6**.

FI$_2$Zr:

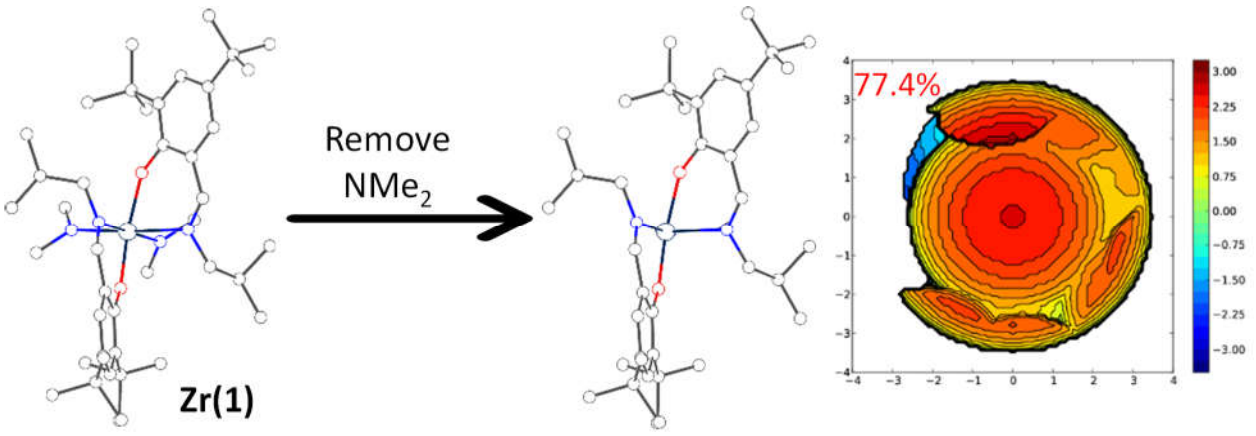

FIZr:

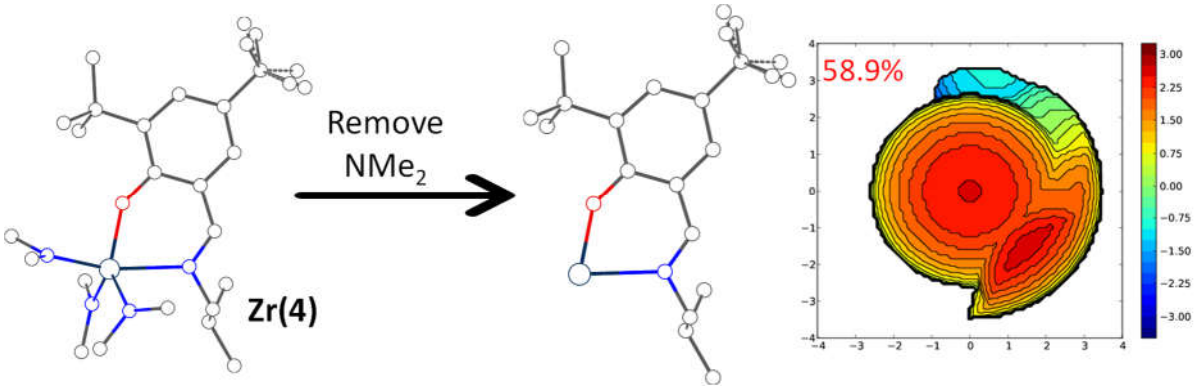

Buried Volume Calculation Results:

	V Free	V Buried	V Total	V Exact	%V_Free	**%V_Bur**	% Tot/Ex
FI_2Zr	40.6	138.9	179.5	179.6	22.6	**77.4**	100.0
FIZr	73.7	105.8	179.5	179.6	41.1	**58.9**	100.0

FI_2Zr:

Quadrant	V_f	V_b	V_t	%V_f	%V_b
SW	13.8	31.0	44.9	30.8	69.2
NW	14.1	30.8	44.9	31.4	68.6
NE	6.1	38.8	44.8	13.5	86.5
SE	6.6	38.2	44.9	14.8	85.2

FIZr:

Quadrant	V_f	V_b	V_t	%V_f	%V_b
SW	26.3	18.6	44.9	58.5	41.5
NW	24.9	20.0	44.9	55.5	44.5
NE	12.4	32.5	44.8	27.6	72.4
SE	10.2	34.7	44.9	22.6	77.4

Polymer Characterization

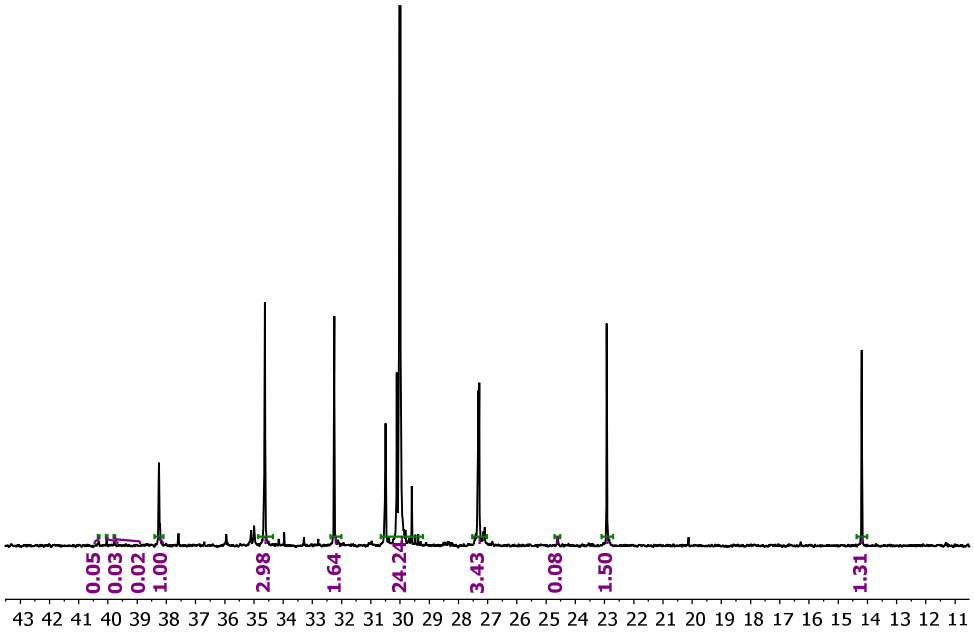

Figure S25. (Table 1, entry 2) ^{13}C NMR spectrum (151 MHz) of poly(ethylene-*co*-1-octene) in 1,1,2,2-tetrachloroethane-d_2 at 120 °C. Reaction conditions: **1** (10 μmol, 1.0 equiv); TMA (0.4 mmol, 40 equiv); BT (12 μmol, 1.2 equiv).

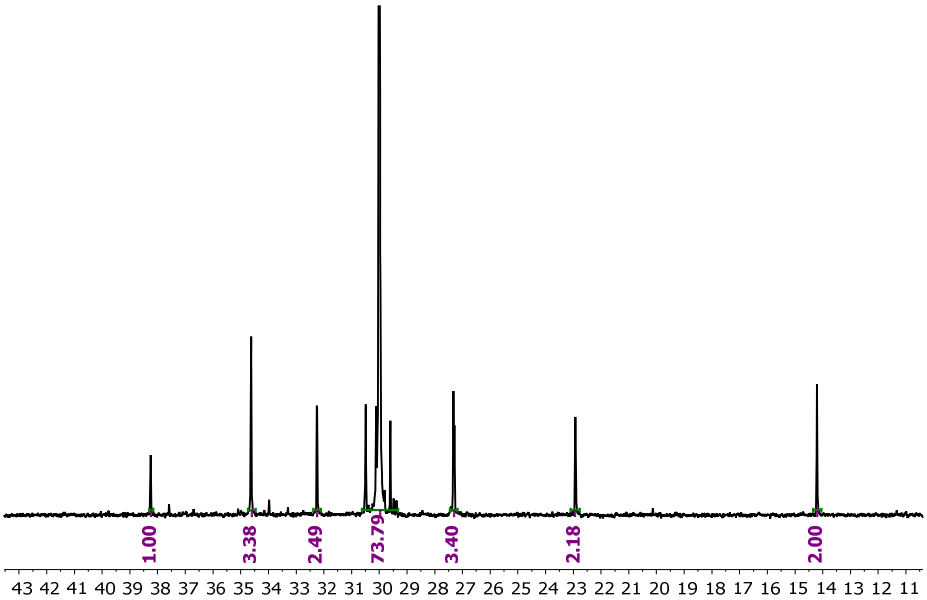

Figure S26. (Table 1, entry 3) ^{13}C NMR spectrum (151 MHz) of poly(ethylene-*co*-1-octene) in 1,1,2,2-tetrachloroethane-d_2 at 120 °C. Reaction conditions: **1** (10 μmol, 1.0 equiv); TMA (1.2 mmol, 120 equiv); BT (12 μmol, 1.2 equiv).

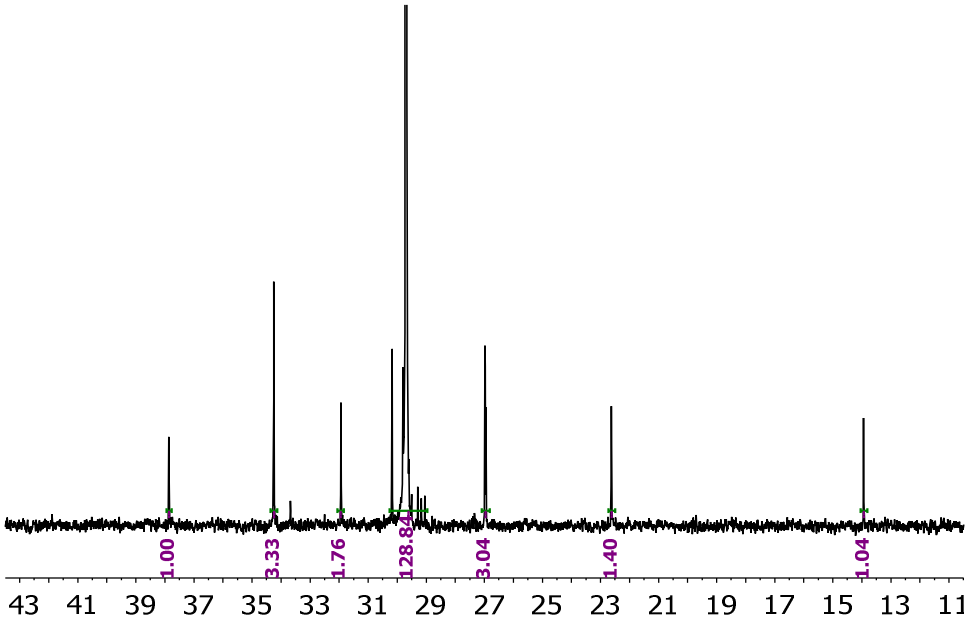

Figure S27. (Table 1, entry 4) ^{13}C NMR spectrum (151 MHz) of poly(ethylene-*co*-1-octene) in 1,1,2,2-tetrachloroethane-d_2 at 120 °C. Reaction conditions: **2** (10 μmol, 1.0 equiv); TMA (0 equiv); BT (12 μmol, 1.2 equiv).

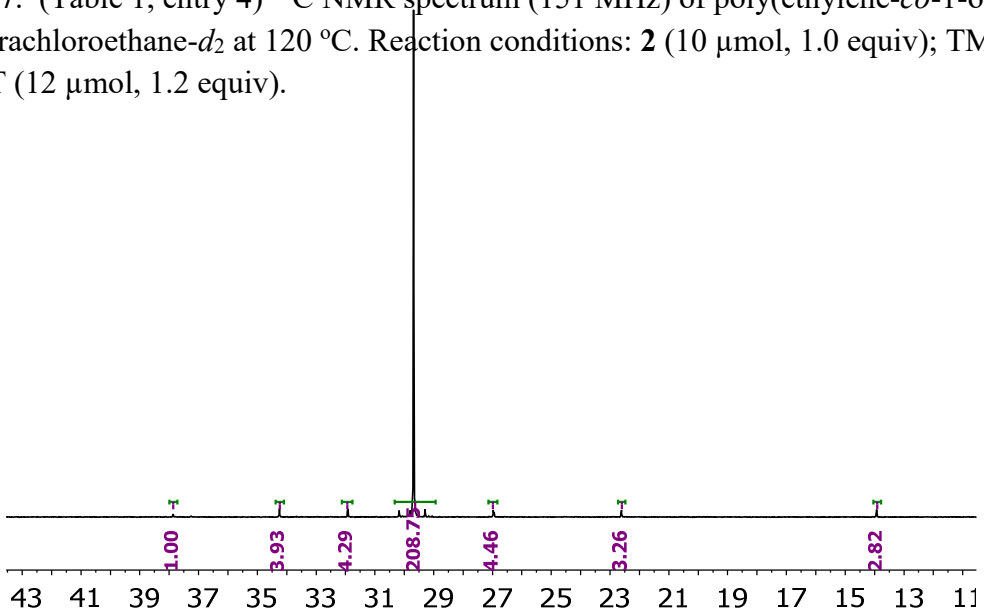

Figure S28. (Table 1, entry 5) ^{13}C NMR spectrum (151 MHz) of poly(ethylene-*co*-1-octene) in 1,1,2,2-tetrachloroethane-d_2 at 120 °C. Reaction conditions: **2** (10 μmol, 1.0 equiv); TMA (0.4 mmol, 40 equiv); BT (12 μmol, 1.2 equiv).

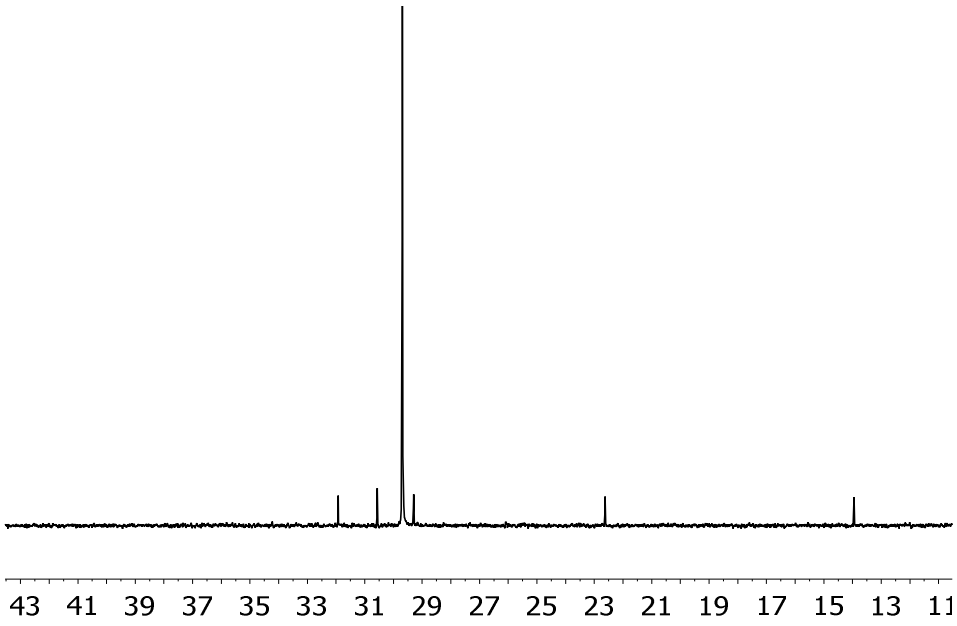

Figure S29. (Table 1, entry 6) ^{13}C NMR spectrum (151 MHz) of poly(ethylene-*co*-1-octene) in 1,1,2,2-tetrachloroethane-d_2 at 120 ºC. Reaction conditions: **2** (10 µmol, 1.0 equiv); TMA (1.2 mmol, 120 equiv); BT (12 µmol, 1.2 equiv).

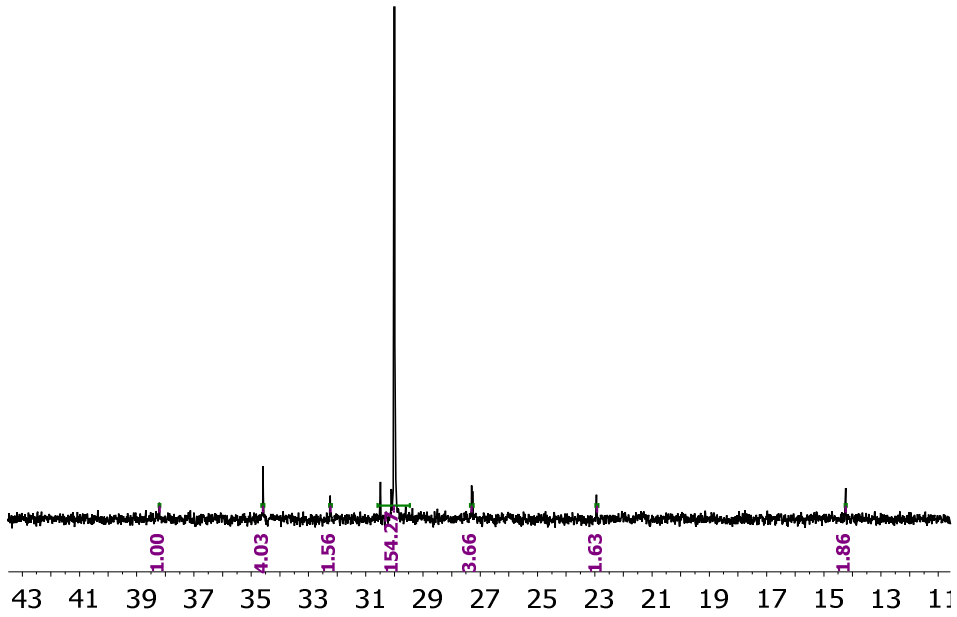

Figure S30. (Table 1, entry 7) ^{13}C NMR spectrum (151 MHz) of poly(ethylene-*co*-1-octene) in 1,1,2,2-tetrachloroethane-d_2 at 120 ºC. Reaction conditions: **3** (10 µmol, 1.0 equiv); TMA (0 equiv); BT (12 µmol, 1.2 equiv).

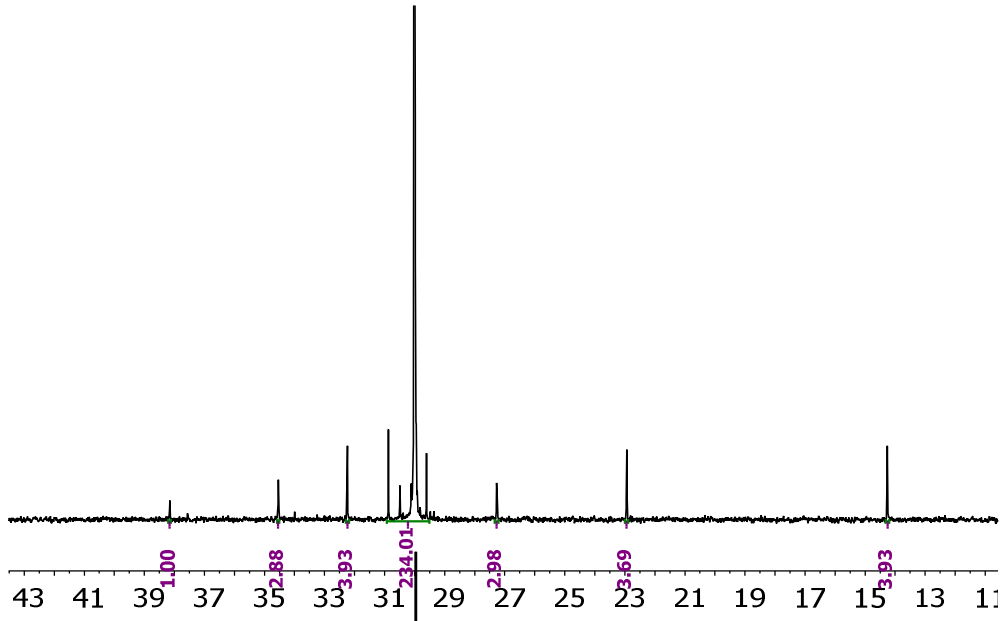

Figure S31. (Table 1, entry 8) ^{13}C NMR spectrum (151 MHz) of poly(ethylene-*co*-1-octene) in 1,1,2,2-tetrachloroethane-d_2 at 120 °C. Reaction conditions: **3** (10 μmol, 1.0 equiv); TMA (0.4 mmol, 40 equiv); BT (12 μmol, 1.2 equiv).

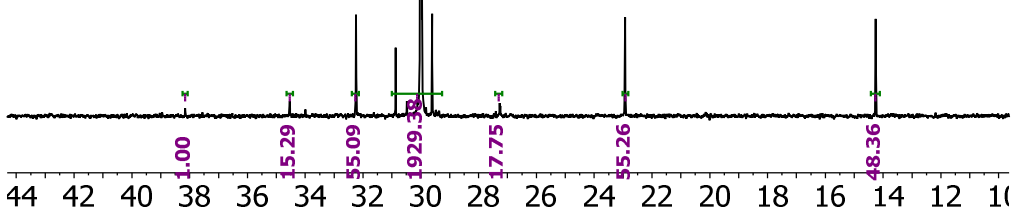

Figure S32. (Table 1, entry 9) ^{13}C NMR spectrum (151 MHz) of poly(ethylene-*co*-1-octene) in 1,1,2,2-tetrachloroethane-d_2 at 120 °C. Reaction conditions: **3** (10 μmol, 1.0 equiv); TMA (1.2 mmol, 120 equiv); BT (12 μmol, 1.2 equiv).

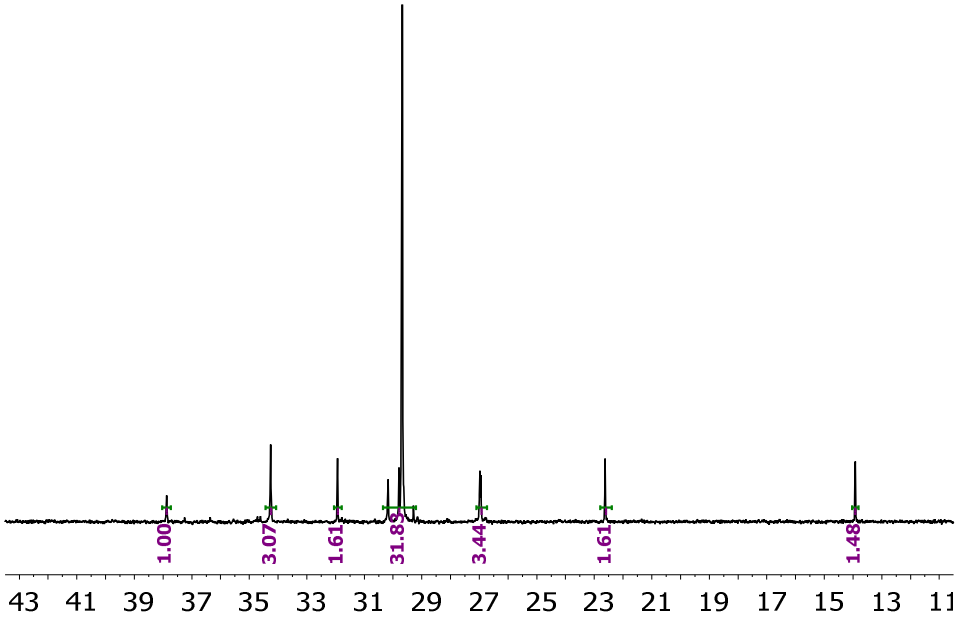

Figure S33. (Table 1, entry 13) ^{13}C NMR spectrum (151 MHz) of poly(ethylene-*co*-1-octene) in 1,1,2,2-tetrachloroethane-d_2 at 120 °C. Reaction conditions: **6** (10 μmol, 1.0 equiv); TMA (0.4 mmol, 40 equiv); BT (12 μmol, 1.2 equiv).

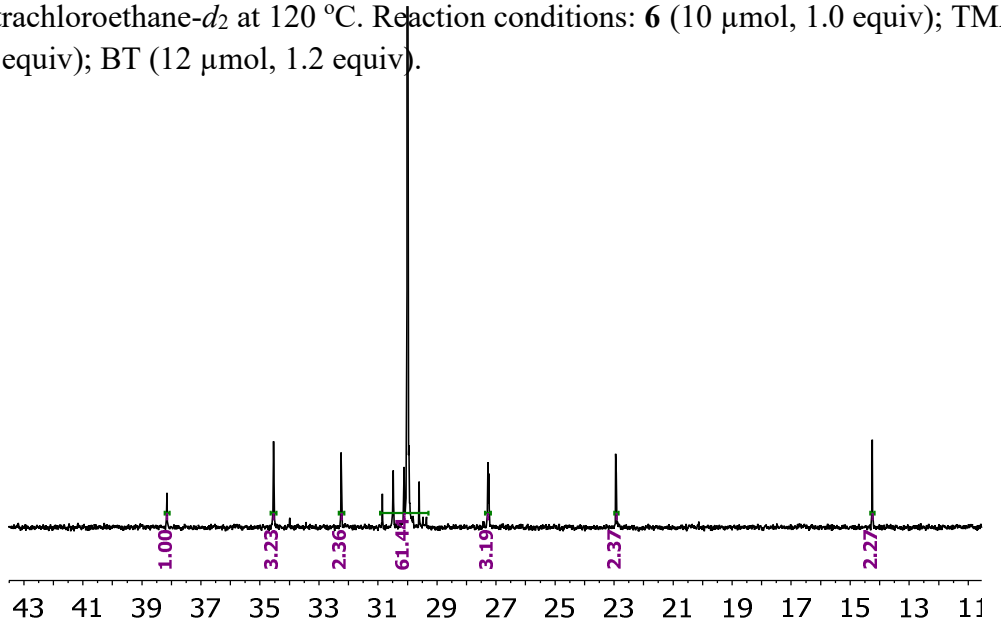

Figure S34. (Table 1, entry 14) ^{13}C NMR spectrum (151 MHz) of poly(ethylene-*co*-1-octene) in 1,1,2,2-tetrachloroethane-d_2 at 120 °C. Reaction conditions: **6** (10 μmol, 1.0 equiv); TMA (1.2 mmol, 120 equiv); BT (12 μmol, 1.2 equiv).

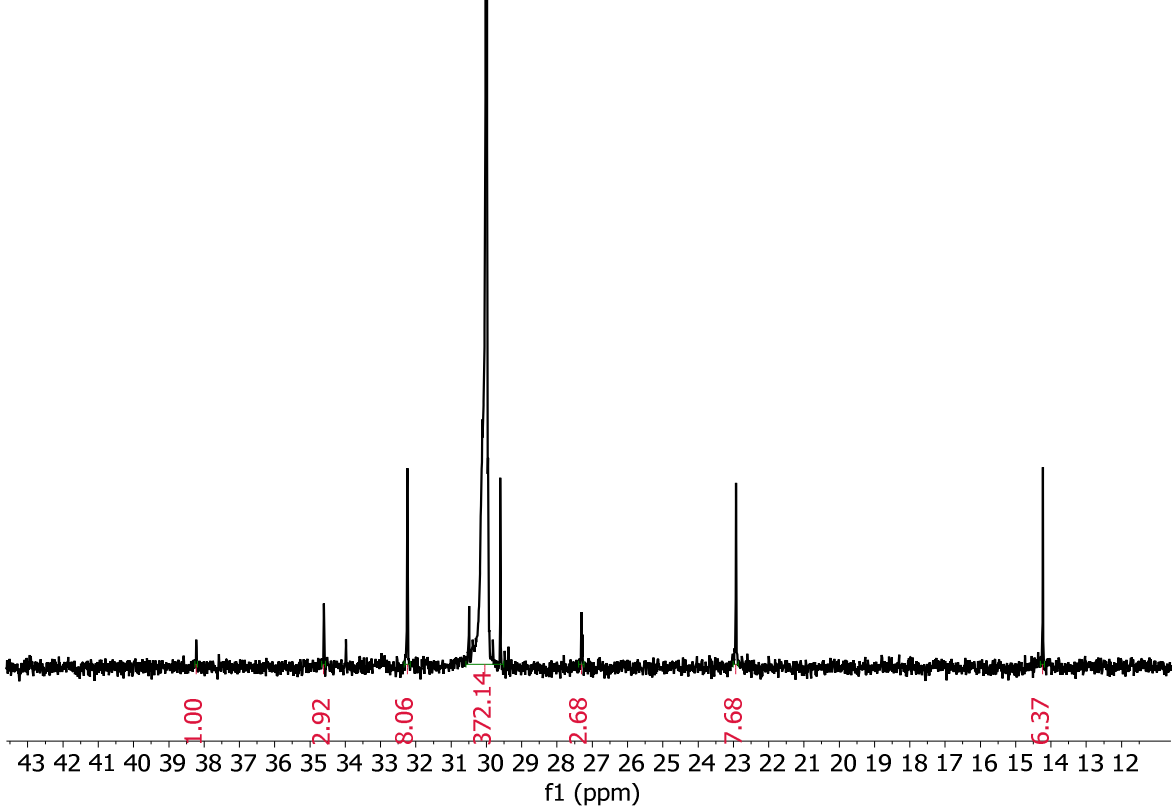

Figure S35. (Table 1, entry 16) ^{13}C NMR spectrum (151 MHz) of poly(ethylene-*co*-1-octene) in 1,1,2,2-tetrachloroethane-d_2 at 120 °C. Reaction conditions: **6** (10 μmol, 1.0 equiv); TMA (1.2 mmol, 120 equiv); $Al_2(NMe_2)_2Me_4$ (10 μmol, 1.0 equiv); BT (12 μmol, 1.2 equiv).

References

1. Pangborn, A. B.; Giardello, M. A.; Grubbs, R. H.; Rosen, R. K.; Timmers, F. J., Safe and Convenient Procedure for Solvent Purification. *Organometallics* **1996,** *15*, 1518-1520.

2. Galland, G. B.; de Souza, R. F.; Mauler, R. S.; Nunes, F. F., ^{13}C NMR Determination of the Composition of Linear Low-Density Polyethylene Obtained with [η^3-Methallyl-nickel-diimine]PF_6 Complex. *Macromolecules* **1999,** *32*, 1620-1625.

3. Zhang, C. M.; Pan, H. Q.; Klosin, J.; Tu, S. Y.; Jaganathan, A., Synthetic Optimization and Scale-Up of Imino-Amido Hafnium and Zirconium Olefin Polymerization Catalysts. *Organic Process Research & Development* **2015,** *19*, 1383-1391.

4. Makio, H.; Prasad, A. V.; Terao, H.; Saito, J.; Fujita, T., Isospecific Propylene Polymerization with *in situ* Generated Bis(phenoxy-amine)zirconium and Hafnium Single Site Catalysts. *Dalton Trans.* **2013,** *42*, 9112-9119.

5. Edson, J. B.; Wang, Z.; Kramer, E. J.; Coates, G. W., Fluorinated Bis(phenoxyketimine)titanium Complexes for the Living, Isoselective Polymerization of

Propylene: Multiblock Isotactic Polypropylene Copolymers via Sequential Monomer Addition. *J. Am. Chem. Soc.* **2008,** *130*, 4968-4977.

6. Fujita, T.; Kawai, K., FI Catalysts for Olefin Oligomerization and Polymerization: Production of Useful Olefin-Based Materials by Unique Catalysis. *Topics in Catalysis* **2014,** *57*, 852-877.

7. Tohi, Y.; Makio, H.; Matsui, S.; Onda, M.; Fujita, T., Polyethylenes with Uni-, Bi-, and Trimodal Molecular Weight Distributions Produced with a Single Bis(phenoxy-imine)zirconium Complex. *Macromolecules* **2003,** *36*, 523-525.

8. Matsui, S.; Mitani, M.; Saito, J.; Tohi, Y.; Makio, H.; Matsukawa, N.; Takagi, Y.; Tsuru, K.; Nitabaru, M.; Nakano, T.; Tanaka, H.; Kashiwa, N.; Fujita, T., A Family of Zirconium Complexes Having Two Phenoxy-Imine Chelate Ligands for Olefin Polymerization. *J. Am. Chem. Soc.* **2001,** *123*, 6847-6856.

9. Lee, C.-L.; Lin, Y.-F.; Jiang, M.-T.; Lu, W.-Y.; Vandavasi, J. K.; Wang, L.-F.; Lai, Y.-C.; Chiang, M. Y.; Chen, H.-Y., Improvement in Aluminum Complexes Bearing Schiff Bases in Ring-Opening Polymerization of ε-Caprolactone: A Five-Membered-Ring System. *Organometallics* **2017,** *36*, 1936-1945.

10. Thomas, C. J.; Krannich, L. K.; Watkins, C. L., Reactivity of $(Me_3Al)_2$ with Selected Aminoarsines and Secondary Amines. *Polyhedron* **1993,** *12*, 389-399.

11. Gowda, R. R.; Chen, E. Y. X., Chiral and Achiral (imino)phenoxy-Based Cationic Group 4 Non-metallocene Complexes as Catalysts for Polymerization of Renewable α-methylene-γ-butyrolactones. *Dalton Trans.* **2013,** *42*, 9263-9273.

12. Sattler, A.; VanderVelde, D. G.; Labinger, J. A.; Bercaw, J. E., Lewis Acid Promoted Titanium Alkylidene Formation: Off-Cycle Intermediates Relevant to Olefin Trimerization Catalysis. *J. Am. Chem. Soc.* **2014,** *136*, 10790-10800.

13. Sattler, A.; Labinger, J. A.; Bercaw, J. E., Highly Selective Olefin Trimerization Catalysis by a Borane-Activated Titanium Trimethyl Complex. *Organometallics* **2013,** *32*, 6899-6902.

14. Mason, A. F.; Coates, G. W., Gel Permeation Chromatography as a Combinatorial Screening Method: Identification of Highly Active Heteroligated Phenoxyimine Polymerization Catalysts. *J. Am. Chem. Soc.* **2004,** *126*, 10798-10799.

15. Yao, E. D.; Wang, J. C.; Chen, Z. T.; Ma, Y. G., Homo- and Heteroligated Salicylaldiminato Titanium Complexes with Different Substituents Ortho to the Phenoxy Oxygens for Ethylene and Ethylene/1-Hexene (Co)polymerization. *Macromolecules* **2014,** *47*, 8164-8170.

16. Pennington, D. A.; Clegg, W.; Coles, S. J.; Harrington, R. W.; Hursthouse, M. B.; Hughes, D. L.; Light, M. E.; Schormann, M.; Bochmann, M.; Lancaster, S. J., The Synthesis, Structure and Ethene Polymerisation Catalysis of Mono(salicylaldiminato) Titanium and Zirconium Complexes. *Dalton Trans.* **2005**, 561-571.

17. Goerl, C.; Betthausen, E.; Alt, H. G., Di- and Trinuclear Iron/Titanium and Iron/zirconium Complexes with Heterocyclic Ligands as Catalysts for Ethylene Polymerization. *Polyhedron* **2016,** *118*, 37-51.

18. Flisak, Z., Theoretical study of isomerism in phenoxyimine-based precursors of coordinative olefin polymerization catalysts. *J. Mol. Catal. A: Chem.* **2010,** *316*, 83-89.

19. Makio, H.; Terao, H.; Iwashita, A.; Fujita, T., FI Catalysts for Olefin Polymerization-A Comprehensive Treatment. *Chem. Rev.* **2011,** *111*, 2363-2449.

20. Zhang, C.; Pan, H.; Klosin, J.; Tu, S.; Jaganathan, A.; Fontaine, P. P., Synthetic Optimization and Scale-up of Imino-Amido Hafnium and Zirconium Olefin Polymerization Catalysts. *Org. Process Res. Dev.* **2015,** *19*, 1383-1391.

21. Dolomanov, O. V.; Bourhis, L. J.; Gildea, R. J.; Howard, J. A. K.; Puschmann, H., OLEX2: a complete structure solution, refinement and analysis program. *J. Appl. Cryst.* **2009,** *42*, 339-341.

22. Sheldrick, G., SHELXT - Integrated Space-Group and Crystal-Structure Determination. *Acta Crystallogr. A* **2015,** *71*, 3-8.

23. Sheldrick, G. M., Crystal Structure Refinement with SHELXL. *Acta Crystallogr. C* **2015,** *71*, 3-8.

24. Thorn, A.; Dittrich, B.; Sheldrick, G. M., Enhanced Rigid-Bond Restraints. *Acta Crystallogr. A* **2012,** *68*, 448-451.

25. Falivene, L.; Credendino, R.; Poater, A.; Petta, A.; Serra, L.; Oliva, R.; Scarano, V.; Cavallo, L., SambVca 2. A Web Tool for Analyzing Catalytic Pockets with Topographic Steric Maps. *Organometallics* **2016,** *35*, 2286-2293.